Stem Cell Reports
Article

ISSCR

OPEN ACCESS

A *miR-590/Acvr2a/Rad51b* Axis Regulates DNA Damage Repair during mESC Proliferation

Qidong Liu,[1] Guiying Wang,[1] Yafang Chen,[1] Guoping Li,[1] Dandan Yang,[1] and Jiuhong Kang[1,*]
[1]Clinical and Translational Research Center of Shanghai First Maternity and Infant Health Hospital, Shanghai Key Laboratory of Signaling and Disease Research, School of Life Science and Technology, Tongji University, 1239 Siping Road, Shanghai 200092, People's Republic of China
*Correspondence: jhkang@tongji.edu.cn
http://dx.doi.org/10.1016/j.stemcr.2014.10.006

SUMMARY

Embryonic stem cells (ESCs) enable rapid proliferation that also causes DNA damage. To maintain genomic stabilization during rapid proliferation, ESCs must have an efficient system to repress genotoxic stress. Here, we show that withdrawal of leukemia inhibitory factor (LIF), which maintains the self-renewal capability of mouse ESCs (mESCs), significantly inhibits the cell proliferation and DNA damage of mESCs and upregulates the expression of *miR-590*. *miR-590* promotes single-strand break (SSB) and double-strand break (DSB) damage repair, thus slowing proliferation of mESCs without influencing stemness. *miR-590* directly targets *Activin* receptor type 2a (*Acvr2a*) to mediate *Activin* signaling. We identified the homologous recombination-mediated repair (HRR) gene, *Rad51b*, as a downstream molecule of the *miR-590/Acvr2a* pathway regulating the SSB and DSB damage repair and cell cycle. Our study shows that a *miR-590/Acvr2a/Rad51b* signaling axis ensures the stabilization of mESCs by balancing DNA damage repair and rapid proliferation during self-renewal.

INTRODUCTION

Embryonic stem (ES) cells derived from the inner cell mass of the blastocyst have been used to understand early embryonic development (Keller, 2005). The notable characteristic of ESCs is self-renewal that is critically involved in the stimulation of rapid proliferation. In fact, rapid proliferation might protect ESCs from external signals inducing differentiation (Ruiz et al., 2011). However, rapid proliferation would be harmful because it causes successive mitotic division with a long S phase in which DNA is replicating most of the time (Fluckiger et al., 2006; Savatier et al., 2002), and the successive rounds of DNA replication causes many replication errors that may lead to DNA damage (Strumberg et al., 2000; Tichy and Stambrook, 2008). In addition, there is no G1 checkpoint in ESCs (White and Dalton, 2005), which might exacerbate DNA damage during rounds of replication without enough time for repair (Hong and Stambrook, 2004). Consistent with these characteristics, there is a high level of double-strand break (DSB) damage, which is the most toxic type of DNA damage (Valerie and Povirk, 2003), and DSB damage is indicated by the γ-H2AX marker (H2AX becomes phosphorylated on serine 139) in both human ES (hES) cells and mouse ES (mES) cells (Banáth et al., 2009; Chuykin et al., 2008; Momcilovic et al., 2010). Similar to irradiated fibroblast cells, normal mESCs also contain a high frequency of single-strand break (SSB) (Chuykin et al., 2008). However, ESCs still have an integrated genome and stable pluripotency during rapid proliferation (Tichy and Stambrook, 2008; Wang et al., 2008). Additionally, the mutation frequency and mitotic recombination frequency are lower in mESCs than in adult somatic or isogenic mouse embryonic fibroblasts cells (Tichy and Stambrook, 2008). Thus, ESCs must have unique regulatory mechanisms that counteract DNA damage both quickly and efficiently.

Transforming growth factor β (TGF-β) signaling is closely related to DNA damage repair regulation (Mitra et al., 2013). Studies have shown that TGF-β signaling can suppress BRCA1-dependent repair of DSBs (Dubrovska et al., 2005). *Activin* A, a member of the TGF-β superfamily of cytokines, interacts with *Activin* type I (*ALK 2*, *ALK 4*, or *ALK 7*) and type II (*Acvr2a* and *Acvr2b*) receptors (Bondestam et al., 1999; Donaldson et al., 1992; Robson et al., 2008), and it participates in DNA damage repair. In premalignant cells, DSB damage results in *Activin* A-dependent induction of *Cox-2*, which is associated with a high level of γ-H2AX (Carlson et al., 2013; Fordyce et al., 2012). In ductal carcinoma, DNA damage response (shorter telomeres and γ-H2AX foci) is also associated with high level of *Activin* A (Fordyce et al., 2012). Additionally, in hESCs, *Activin* A can maintain pluripotency even without feeder layers (Beattie et al., 2005). In mESCs, *Activin* A signaling can promote cell proliferation (Ogawa et al., 2007). However, it remains unknown whether the maintenance of a stable status in ESCs is also related to the DNA damage repair function of *Activin* A signaling.

DSB damage is the most toxic type of DNA damage (Valerie and Povirk, 2003). Homologous recombination-mediated repair (HRR) is thought to be used in ESCs to repair DSBs (Hasty et al., 1992; Shrivastav et al., 2008; Smih et al., 1995; Tichy et al., 2010). *Rad51* family members, including *Rad51*, *Rad51b*, *Rad5c*, *Rad51d*, and so on, are evolutionarily conserved proteins that play important roles

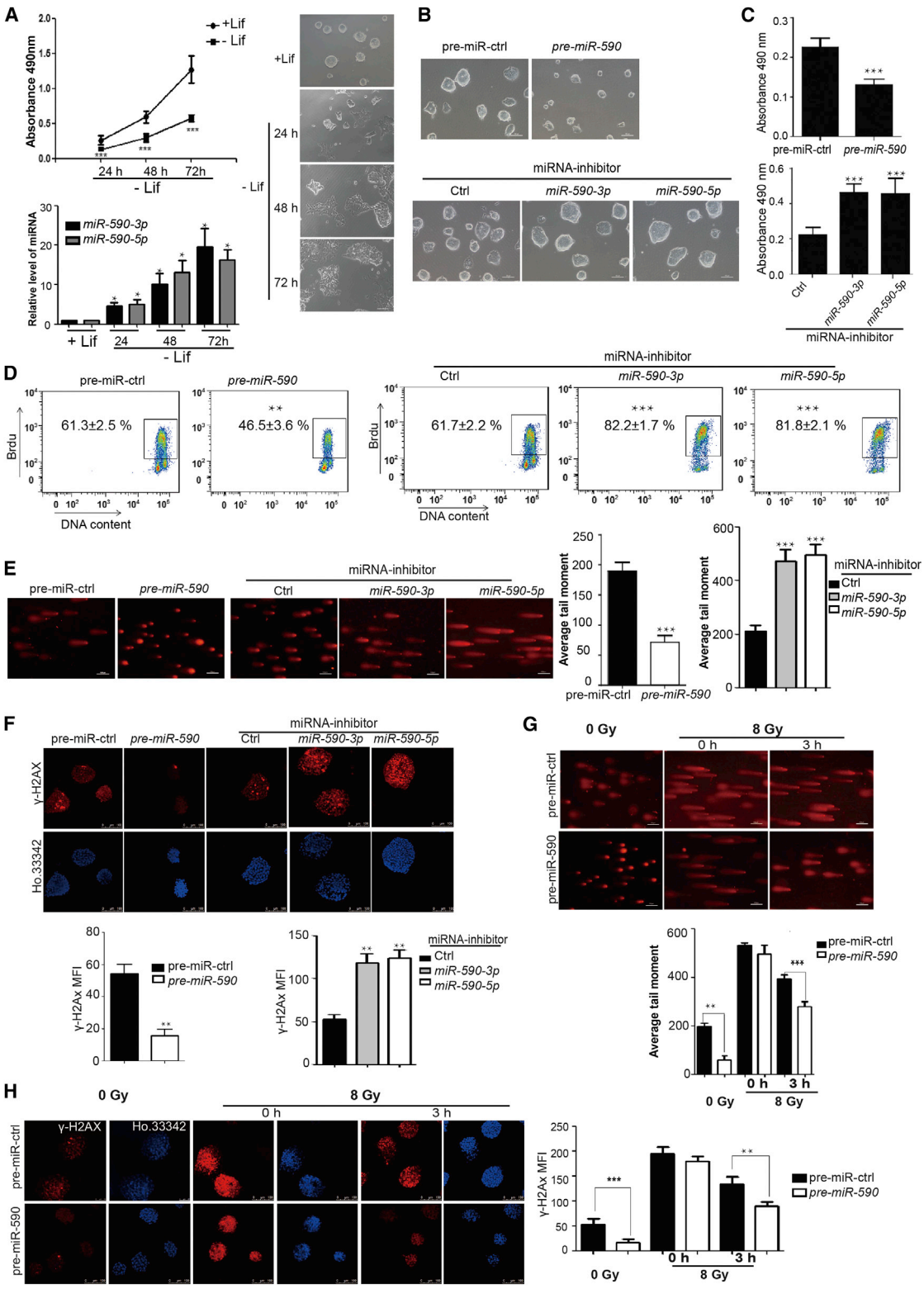

Figure 1. *miR-590* Inhibits Rapid Proliferation and Promotes SSB and DSB Damage Repair of mESCs

(A) Analysis of the proliferation of mESCs cultured with or without LIF by MTS cell proliferation assay. (Bottom) The qRT-PCR verification of *miR-590-3p* and *miR-590-5p* levels. (Right) The morphology of mESCs cultured with (+LIF) on 24 hr or without LIF (−LIF) on 24, 48, 72 hr.

(legend continued on next page)

during HHR (Baumann et al., 1996; Chun et al., 2013; Kawabata et al., 2005; Thacker, 2005). *Rad51* paralogs take part in SSB and DSB damage repair (Jensen et al., 2010, 2013). RAD51B is also a protein kinase regulating the function of cell cycle-related genes (Havre et al., 2000) and is a known molecule to promote HRR by participating in the Holliday junction process (Kawabata et al., 2005; Takata et al., 2000). Previous studies have shown that overexpression of *Rad51b* in Chinese hamster ovary cells causes a G1 delay and UV irradiation hypersensitivity (Havre et al., 1998). TGF-β signaling has also been reported to inhibit DNA damage repair by downregulating the expression of *Rad51* in Mv1Lu epithelial cells (Kanamoto et al., 2002). However, it is unknown whether *Rad51* paralogs can regulate both the DNA damage repair and cell cycle or even maintain their balance in mESCs. Additionally, the upstream regulators of *Rad51* paralogs in mESCs are unclear.

MicroRNAs (miRNAs) are posttranscriptional modulators of gene expression and are connected to the transcriptional regulatory circuitry of mESCs (Marson et al., 2008). Several miRNAs target DNA repair-related factors and influence DNA damage repair. Studies have shown that UV damage promotes miRNA expression in a partially ataxia telangiectasia mutated kinase (ATM)/ataxia telangiectasia and Rad3-related kinase-independent manner (Pothof et al., 2009). Overexpression of *miR-24* attenuates H2AX, leading to high sensitivity to irradiation and reduced repair capacity (Lal et al., 2009). miRNAs can also regulate TGF-β signaling. *miR-302/367* can modulate BMP signaling, which supports self-renewal by targeting BMP inhibitors in hESCs (Lipchina et al., 2011; Qi et al., 2004). However, there is limited understanding of miRNA modulation of these signaling pathways to regulate DNA damage repair to maintain self-renewal during ESC proliferation, which differs from differentiated cells (Tichy and Stambrook, 2008). In the present study, we found that *miR-590* inhibits *Activin* signaling by directly targeting *Acvr2a* to inhibit the expression of *Rad51b*, balancing the DNA damage repair and rapid proliferation of ESCs.

RESULTS

miR-590 Promotes SSB and DSB Damage Repair during Rapid Proliferation of mESCs

Consistent with that, leukemia inhibitory factor (LIF) is critically needed for the self-renewal of mESCs. We found that the rapid proliferation was greatly inhibited in both the cells cultured without LIF, which detected by 3-(4,5-dimethylthiazol-2-yl)-5-(3-carboxymethoxyphenyl)-2-(4-sulfophenyl)-2H-tetrazolium (MTS) assay (Figure 1A) and those during the embryonic body (EB) formation, which detected by flow cytometric (FACS) analysis of 5′-bromodeoxyuridine (BrdU) incorporation (Figure S1A available online). We further found that both of the mature *miR-590*, namely *miR-590-3p* and *miR-590-5p*, were upregulated in cells during the culture without LIF (Figure 1A) and EB formation (Figure S1B), indicating a possible linkage between *miR-590* expression and the mESC proliferation. In order to detect that whether *miR-590* is associated with the regulation of self-renewal, we transfected pre-*miR-590*, which can be processed to be *miR-590-3p* and *miR-590-5p* (Figure S1C), into mESCs and found that the size of mESC colonies became smaller than control cells

Data shown are means ± SD of six independent experiments (n = 6). *p < 0.05, **p < 0.01, and ***p < 0.001. The scale bar represents 100 μm.

(B) Morphology of colonies of mESCs after transfection with pre-*miR-590* or *miR-590-3p/5p* inhibitor. pre-miR-ctrl indicates pre-miRNA control, which has no homology to any known mammalian gene. Inhibitor control is a random sequence molecule that has no homology to any known mammalian gene. The scale bar represents 100 μm.

(C) Analysis of the proliferation of mESCs transfected with pre-*miR-590* or *miR-590-3p/5p* inhibitor by MTS cell proliferation assay. Data shown are means ± SD of five independent experiments (n = 5). ***p < 0.001.

(D) Analysis of the proliferation of mESCs transfected with pre-*miR-590* or *miR-590-3p/5p* inhibitor by FACS analysis of BrdU incorporation. The figure shows the percentage (%) of population the of BrdU-positive cells. Data shown are means ± SD of three independent experiments (n = 3). **p < 0.01 and ***p < 0.001.

(E) Comet assay for SSB damage in mESCs. The scale bar represents 100 μm. Data shown are means ± SD of three independent experiments (n = 3). (Right) The quantification of the average DNA tail moment. ***p < 0.001.

(F) Immunofluorescence analysis of γ-H2AX (red) to indicate the state of DSB damage in mESCs. Ho.33342 (Hoechst 33342) represents nuclear staining (blue). The scale bar represents 100 μm. (Bottom) The quantification of the fluorescence of γ-H2AX immunostaining. Data shown are means ± SD of three independent experiments (n = 3). **p < 0.01. MFI, mean fluorescence intensity.

(G) Comet assay for SSB damage of mESCs with irradiation from X-ray. 0 Gy indicates mESCs not subjected to X-ray irradiation. The scale bar represents 100 μm. The bottom shows the quantification of the average DNA tail moment. Data shown are means ± SD of three independent experiments (n = 3). **p < 0.01 and ***p < 0.001.

(H) Immunofluorescence analysis of γ-H2AX (red) with Ho.33342 (Hoechst 33342) nuclear staining (blue). The scale bar represents 100 μm. (Right) The quantification of the fluorescence of γ-H2AX immunostaining. Data shown are means ± SD of three independent experiments (n = 3). **p < 0.01 and ***p < 0.001.

examined at 48 hr posttransfection (Figure 1B). We further digested mESC clones by trypsin into single cells and counted the amount of the total cells under the microscope by using blood count board and found that total cells transfected with pre-*miR-590* were less than control cells (Figure S1D). Transfection of *miR-590-3p* or *miR-590-5p* mimics respectively into mESCs also resulted in a similar phenomenon of pre-*miR-590* (Figure S1E). In contrast, clone size of mESCs was larger than control cells after transfected with *miR-590-3p* or *miR-590-5p* inhibitor, which can compete for the *miR-590* with target mRNAs (Figure 1B). The amount of total cells was also more than control cells (Figure S1D). MTS assay and FACS of BrdU incorporation also showed that *miR-590* inhibited proliferation of mESCs posttransfected for 48 hr with pre-*miR-590*, while cells transfected with *miR-590-3p* or *miR-590-5p* inhibitor showed faster proliferation than control cells (Figures 1C and 1D). Further, we found that the size of clones of another kind of mESC line 46C after transfected with pre-*miR-590* was also smaller than control mESCs (Figure S1F).

FACS analysis of cell cycle showed that there was a significant reduction in the proportion of cells in S phase and an increase in the proportion of cells in G1 and G2/M phases in mESCs after transfected with pre-*miR-590* for 48 hr (Figure S1G). In contrast, the proportion of cells in S phase was increased and in G1 and G2/M phases was reduced in mESCs transfected with *miR-590-3p* or *miR-590-5p* inhibitor (Figure S1G). *miR-590* could not induce the apoptosis (Figure S1H) and showed no significant influence on the expression of stemness genes (Figure S1I).

Additionally, we found that *miR-590* can regulate the SSB and DSB damage in mESCs. SSB and DSB damage was relieved in mESCs after being transfected with pre-*miR-590* detected by the comet assay and the immunostaining of γ-H2AX foci, respectively (Figures 1E and 1F). In contrast, mESCs transfected with the *miR-590-3p* or *miR-590-5p* inhibitor showed increased SSB damage (Figure 1E) and DSB (Figure 1F). To investigate whether *miR-590* can promote DNA damage repair directly or through regulating proliferation to free up more time to repair DNA, we used X-ray to irradiate mESCs to simulate DSB and SSB damage. We found that after treating with 8 Gy radiation, both mESCs transfected with pre-*miR-590* and pre-miR-control showed violent DSB and SSB damage. Three hours later, both groups of mESCs had repaired much DNA damage (Figures 1G and 1H). However, we found that the repair capacity of mESCs transfected with pre-*miR-590* was faster than that of control mESCs. The DNA damage was significantly decreased in mESCs transfected with pre-*miR-590* compared with control mESCs (Figures 1G and 1H). Trypan blue staining showed that there was no significant dying cell in mESCs after transfected with pre-*miR-590* or 0/3 hr postirradiated by 8 Gy X-ray (Figures S1J and S1K). Thus, we concluded that *miR-590* may regulate DNA damage repair directly in mESCs. Additionally, the *miR-590* regulation of proliferation led us to investigate whether *miR-590* connects the cell proliferation and DNA damage repair in mESCs.

miR-590 Regulates the Expression of *Rad51b* and Cell Cycle-Related Genes

To test whether cell cycle-related, SSB damage repair-related, and DSB damage repair-related genes can be regulated by *miR-590*, we performed quantitative RT-PCR (qRT-PCR) and western blot analyses examined 48 hr posttransfection, and we found that *Rad51b* was upregulated in mESCs transfected with pre-*miR-590* but that *Rad51c*, *Rad9*, and *Brca1* showed no significant change (Figure 2A). Additionally, the cell cycle-related genes, *Cyclin E* and *Cyclin B*, were downregulated while *P21* and *Rb1* were upregulated (Figure 2A). Western blot analysis was used to confirm the change in protein levels of the cell cycle-related genes and *Rad51b* (Figure 2B). In contrast, the *miR-590-3p* or *miR-590-5p* inhibitor downregulated the expression of *Rad51b*, *p21*, and *Rb1* and upregulated the expression of *Cyclin B* and *Cyclin E* (Figure 2C). Protein levels of the cell cycle-related genes and *Rad51b* were detected to confirm the function of *miR-590-3p* or *miR-590-5p* inhibitors (Figure 2D). These results showed that *miR-590* may mediate downstream genes to regulate DSB damage repair, SSB damage repair, as well as the cell proliferation.

miR-590 Directly Targets *Acvr2a* to Regulate *Activin* Signaling in mESCs

We used Targetscan and Miranda to predict the direct target of miRNAs and found that both *miR-590-3*p and *miR-590-5p* can target *Acvr2a* (Figure 3A). Then we found that *Acvr2a* was downregulated in mESCs cultured without LIF compared with mESCs cultured with LIF (Figure 3A), which was opposite to the upregulation of *miR-590 −3p/5p* in the mESCs cultured in the same system (Figure 1A). These results thus suggested a negative correlation between *Acvr2a* and *miR-590-3p/5p* during the differentiation of mESCs. Furthermore, we performed luciferase reporter assay to analyze whether *miR-590-3p* or *miR-590-5p* can target the 3′UTR of *Acvr2a* mRNA. We generated WT and mutant 3′UTR reporters of *Acvr2a* and found that both *miR-590-3p* and *miR-590-5p* inhibited the luciferase activity of the WT 3′UTR reporter but not the mutant reporters (Figure 3B). Furthermore, we detected *miR-590* regulation on endogenous *Acvr2a* in mESCs. We transfected pre-*miR-590* into mESCs and found that the expression of *Acvr2a* on both the mRNA and protein level was decreased (Figure 3C). To investigate whether miR-590 can influence *Activin* signaling, we detected the level of p-SMAD2 by western blot analysis and found that mESCs transfected with

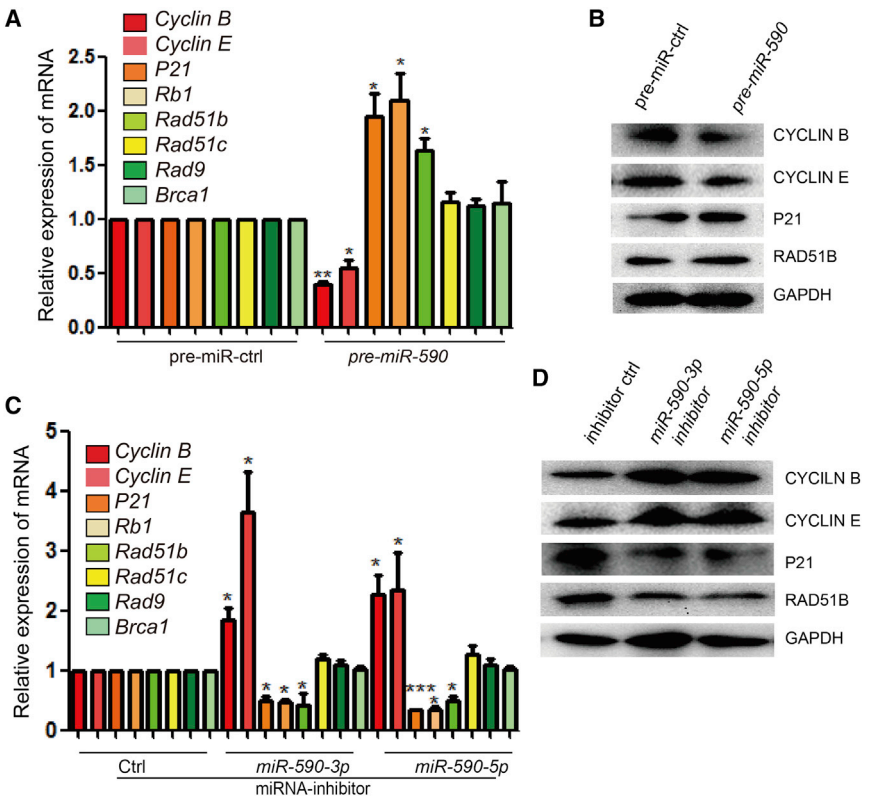

Figure 2. Effects of *miR-590* on Cell Cycle and DNA Damage Repair-Related Genes

(A) qRT-PCR verification of transcript levels of the cell cycle regulation and homologous recombination damage repair genes in mESCs transfected with pre-*miR-590* or control. Data shown are means ± SD of three independent experiments (n = 3). *p < 0.05 and **p < 0.01.

(B) Western blot analysis for the cell cycle regulation and homologous recombination damage repair genes in mESCs transfected with pre-*miR-590* or control.

(C) qRT-PCR verification of mRNA levels of the cell cycle regulation and homologous recombination damage repair genes in mESCs transfected with *miR-590-3p/5p* inhibitor or control. Data shown are means ± SD of three independent experiments (n = 3). *p < 0.05 and ***p < 0.001.

(D) Western blot analysis of the cell cycle regulation and homologous recombination damage repair genes in mESCs transfected with *miR-590-3p/5p* inhibitor or control.

pre-*miR-590* had a lower level of p-SMAD2 than the control group (Figure 3D). Transfection of the *miR-590-3p* or *miR-590-5p* inhibitor increased the level of p-SMAD2 (Figure 3E). These results demonstrated that *miR-590* inhibits the *Activin* signaling pathway by directly targeting *Acvr2a*.

The *miR-590/Acvr2a* Pathway Balances SSB and DSB Damage Repair with Rapid Proliferation of mESCs

We next tested whether the *miR-590/Acvr2a* pathway can regulate mESC proliferation and DNA damage repair. We constructed the *Acvr2a* overexpression vector (Figure S2A). Then we found that clone size of mESCs overexpressed *Acvr2a* was larger than control cells (Figure 4A). The amount of total cells was also more than control cells (Figure S2B). Both the FACS analysis of BrdU incorporation and MTS assay showed the increase of proliferation of mESCs overexpressed by *Acvr2a* (Figures 4B and 4C). FACS analysis of cell cycle showed that there was a significant increase in the proportion of cells in S phase and a reduction in the proportion of cells in G1 and G2/M phases in mESCs overexpressed by *Acvr2a* examined at 48 hr posttransfection (Figure S2C).

We also found that overexpression of *Acvr2a* caused more SSB (Figure 4D) and DSB damage (Figure 4E) in mESCs compared with the control mESCs, and the overexpression of *Acvr2a* increased the expression of *Cyclin B* and *Cyclin E* as well as decreased the expression of *Rad51b*, *P21*, and *Rb1* (Figure 4F). As expected, in mESCs with *Acvr2a* knockdown, clone size is smaller than control cells (Figure S2D). The amount of total cells was also less than control group (Figure S2D). Proliferation was inhibited by downregulation of the protein level of *Acvr2a* (Figure S2E). There was a significant reduction in the proportion of cells in S phase and an increase in the proportion of cells in G1 and G2/M phases in mESCs with downregulation of *Acvr2a* (Figure S2F). The SSB and DSB damage were also decreased in mESCs with knockdown of *Acvr2a* (Figures S2G and S2H).

We next tested whether *miR-590* can regulate the DSB, SSB damage repair, and cell proliferation of mESCs by directly targeting *Acvr2a*. We performed a rescue experiment. The expression level of *Acvr2a* was detected by qPCR in rescue experiment. We first detected the *Acvr2a* expression level of the rescue experiment (Figure S3A) and found that the influence on clone size (Figure 4G), cell proliferation ((Figures 4H, 4I, and S3B), and cell cycle (Figure S3C) of mESCs transfected with pre-*miR-590* could be restored by overexpressing *Acvr2a*. We also showed that overexpression of *Acvr2a* in mESCs transfected with pre-*miR-590* could restore the state of excessive SSB and DSB DNA damage (Figures 4J and 4K) to a similar level of control mESCs. The cell cycle-related genes and *Rad51b* were also restored by overexpressing *Acvr2a* in mESCs transfected with pre-*miR-590* (Figure 4L). These results showed that *miR-590* regulated the DNA damage repair and cell proliferation of mESCs through directly targeting *Acvr2a*.

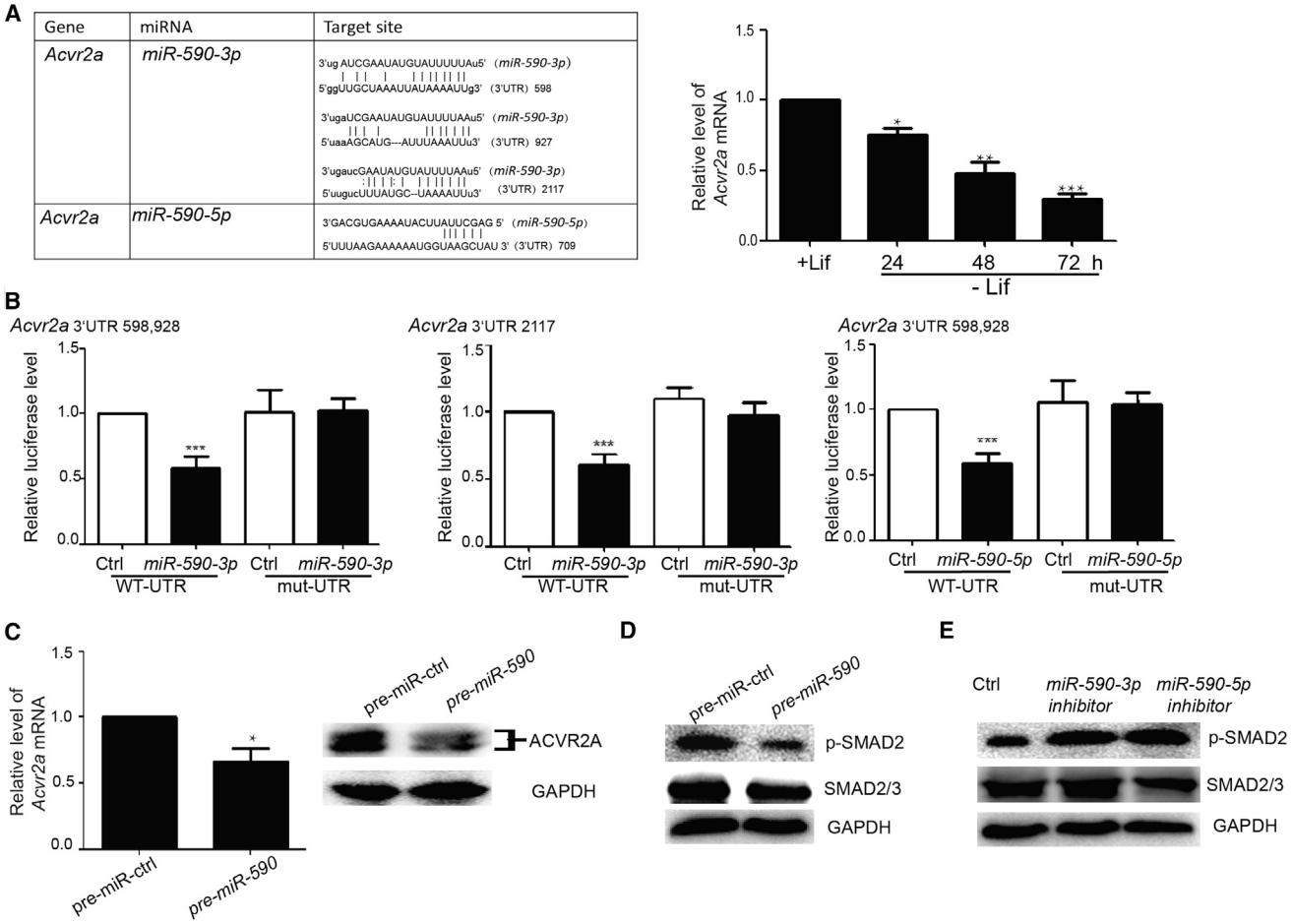

Figure 3. *miR-590* Directly Targets *Acvr2a* to Regulate *Activin* Signaling in mESCs

(A) Summary of *miR-590-3p* and *miR-590-5p* target sites in the 3′UTRs of *Acvr2a*. In the double strands of the sequence, the upper strand is *miR-590-3p* or *miR-590-5p*, and the lower strand is the binding sites of 3′UTR mRNA. The right panel shows the level of *Acvr2a* expression detected by qRT-PCR. Data shown are means ± SD of three independent experiments (n = 3). *p < 0.05, **p < 0.01, and ***p < 0.001.

(B) *miR-590-3p* and *miR-590-5p* specifically repress their targets in the luciferase assay. WT-UTR indicates WT 3′ UTR. Mut-UTR indicates the 3′UTR containing the mutant binding site of *miR-590*. Data shown are means ± SD of three independent experiments (n = 3). ***p < 0.001.

(C) Detection of *Acvr2a* expression on mRNA and protein levels in mESCs. Data shown are means ± SD of three independent experiments (n = 3). *p < 0.05.

(D and E) The level of p-SMAD2 was detected by western blot analysis. Glyceraldehyde-3-phosphate dehydrogenase is as an internal control.

Rad51b Promotes SSB and DSB Damage Repair in mESCs to Slow the Cell Proliferation

We found that *Rad51b* can be regulated by the *miR-590/Acvr2a* pathway. To determine whether *Rad51b* can inhibit the mES proliferation and repair SSB and DSB damage, we downregulated the expression of *Rad51b* in mESCs. The colonies of mESCs with knockdown of *Rad51b* were larger than control cells (Figure 5A). The total number of cells was more than control cells (Figure S4A). The proliferation was increased by downregulating *Rad51b* in mESCs detected by MTS assay and FACS analysis of BrdU incorporation (Figures 5B and 5C). We also found that knockdown of *Rad51b* resulted in a reduced fraction of cells in G1 and G2/M phases as well as an increased fraction of cells in S phase (Figure S4B). The SSB and DSB damage was significantly increased after knockdown of *Rad51b* (Figures 5D and 5E). In mESCs with *Rad51b* knockdown, the expression levels of *Cyclin B* and *Cyclin E* were upregulated, and the expression levels of *P21* and *Rb1* were downregulated (Figure 5F). These results showed that *Rad51b* can regulate both the DNA damage repair and cell proliferation in mESCs to balance the rapid proliferation and DNA damage repair.

The *miR-590/Acvr2a/Rad51b* Pathway Balances the Rapid Proliferation and DNA Damage Repair of mESCs

To confirm whether *Rad51b* is the functional component of the *miR-590/Acvr2a* pathway, we performed rescue experiments. We downregulated the expression of *Rad51b* in mESCs transfected with pre-*miR-590* and found that the size of clones (Figure 6A) and amount of total cells (Figure S5A) were restored compared with mESCs transfected only with pre-*miR-590*. MTS assay and BrdU incorporation assay showed the rapid proliferation of mESCs was restored by downregulating *Rad51b* compared with mESCs transfected only with pre-*miR-590* (Figures 6B and 6C). FACS analysis of cell cycle showed that the fraction of cell cycle in mESCs with exogenous pre-*miR-590* transfection was restored by knockdown of *Rad51b* (Figure S5B). The state of SSB and DSB damage in mESCs transfected with pre-*miR-590* was also restored by knockdown of *Rad51b* (Figures 6D and 6E). The levels of cell cycle-related genes and *Rad51b* in the rescue group were similar to those in the control group (Figure 6F). These results showed that *Rad51b* is the downstream functional factor of *miR-590* and regulates both DNA damage and cell proliferation.

Furthermore, we performed a rescue experiment to test the regulation of *Rad51b* by *Acvr2a*. We found that knockdown of *Rad51b* restored the size of clones and the amount of total cells of mESCs with *Acvr2a* knockdown (Figures 6G and S5C). Additionally, the capacity of proliferation (Figures 6H and 6I) and fraction of cell cycle (Figure S5D) in *Acvr2a* knockdown mESCs was also restored after downregulation of *Rad51b*.

We also found that downregulation of *Rad51b* restored the DSB and SSB damage in *Acvr2a* knockdown mESCs, which was similar to the control mESCs (Figures 6J and 6K). The expression levels of cell cycle-related genes and Rad51B were restored to similar level of the control group (Figure 6L). These results confirmed that *Rad51b* is a downstream functional factor of *Acvr2a* and that the *miR-590/Acvr2a/Rad51b* pathway balances the rapid proliferation with DSB and SSB damage repair in mESCs to maintain the self-renewal and genome integrity.

DISCUSSION

Rapid proliferation can maintain the self-renewal of ESCs, but it can also result in DNA damage that leads to catastrophic mutations affecting the differentiation of organisms and causing mutations to be passed to progeny (Savatier et al., 2002; Tichy and Stambrook, 2008). In response to DNA damage stress, cells generally slow or arrest cell cycle progression to repair or prevent the transmission of damage to daughter cells (Ishikawa et al., 2006). Cell cycle and DNA damage repair can be regulated during mES differentiation. During differentiation, mESCs accumulate in G1 phase and exhibit a cell cycle lengthened from 8–10 hr to more than 16 hr (White and Dalton, 2005). Additionally, DNA damage, especially DSB damage, is decreased during differentiation (Turinetto et al., 2012). Thus, there should be a system balancing the paradox of rapid proliferation and DNA damage repair to guarantee the normal self-renewal, pluripotency, and genomic stabilization in ESCs (Tichy, 2011). Here, we found that *miR-590* balances DNA damage repair and proliferation by affecting the expression of *Rad51b* in mESCs. Importantly, *Activin* signaling regulated by *Acvr2a* mediates the balancing regulation of *miR-590* on *Rad51b*. Furthermore, the *miR-590/Acvr2a/Rad51b* axis regulates the balance of rapid proliferation and DNA damage repair in mESCs.

The DNA damage repair system involves a complex network in which miRNAs play important roles (Chen and Rajewsky, 2007; Song et al., 2011; Wan et al., 2011). For example, *miR-24* and *miR-138* can downregulate H2AX, leading to high sensitivity to radiation and weak repair capacity (Lal et al., 2009). *miR-182* suppresses DSB damage repair by targeting *Brca1* (Moskwa et al., 2011). A previous study has also shown that *miR-590* participates in the regulation of cell proliferation and death. *miR-590-3p* regulates neuronal death in patients with Alzheimer disease and frontotemporal lobar degeneration (Villa et al., 2011). In bladder cancer, *miR-590-3p* inhibits cell proliferation and migration (Mo et al., 2013). In acute myeloid leukemia, *miR-590-5p* can be regulated by interleukin-3 to affect the growth of cells (Favreau and Sathyanarayana, 2012). These studies suggest that *miR-590* widely participates in cell growth of different cell types. However, the function of *miR-590* in mESCs remains unknown. We found that overexpression of *miR-590* significantly inhibited the proliferation by upregulating the expression of *P21* and *Rb1* as well as downregulating the expression of *Cyclin E* and *Cyclin B*, but the overexpression of *miR-590* did not affect the pluripotency of mESCs. This result was similar to that of a previous study where no significant induction of differentiation of mESCs occurred with overexpression of *P21* and *Rb* (Li et al., 2012). LIF signaling is important for mESCs to maintain rapid proliferation (Furue et al., 2005). In our study, we also found that during the process of culture withdrawing LIF, the proliferation rate of mESCs was slower, and *miR-590-3p/5p* were upregulated, suggesting a possible important role of *miR-590* during mESC proliferation regulation. Studies have shown that ESCs have robust DNA damage repair capacity, which includes nucleotide excision repair (Saretzki et al., 2004), mismatch repair (Saretzki et al., 2004), and DSB repair (Donoho et al., 1998; Smih et al., 1995). DSB damage is considered to be the most toxic type of DNA damage (Valerie and Povirk, 2003), which may be caused by the replication fork

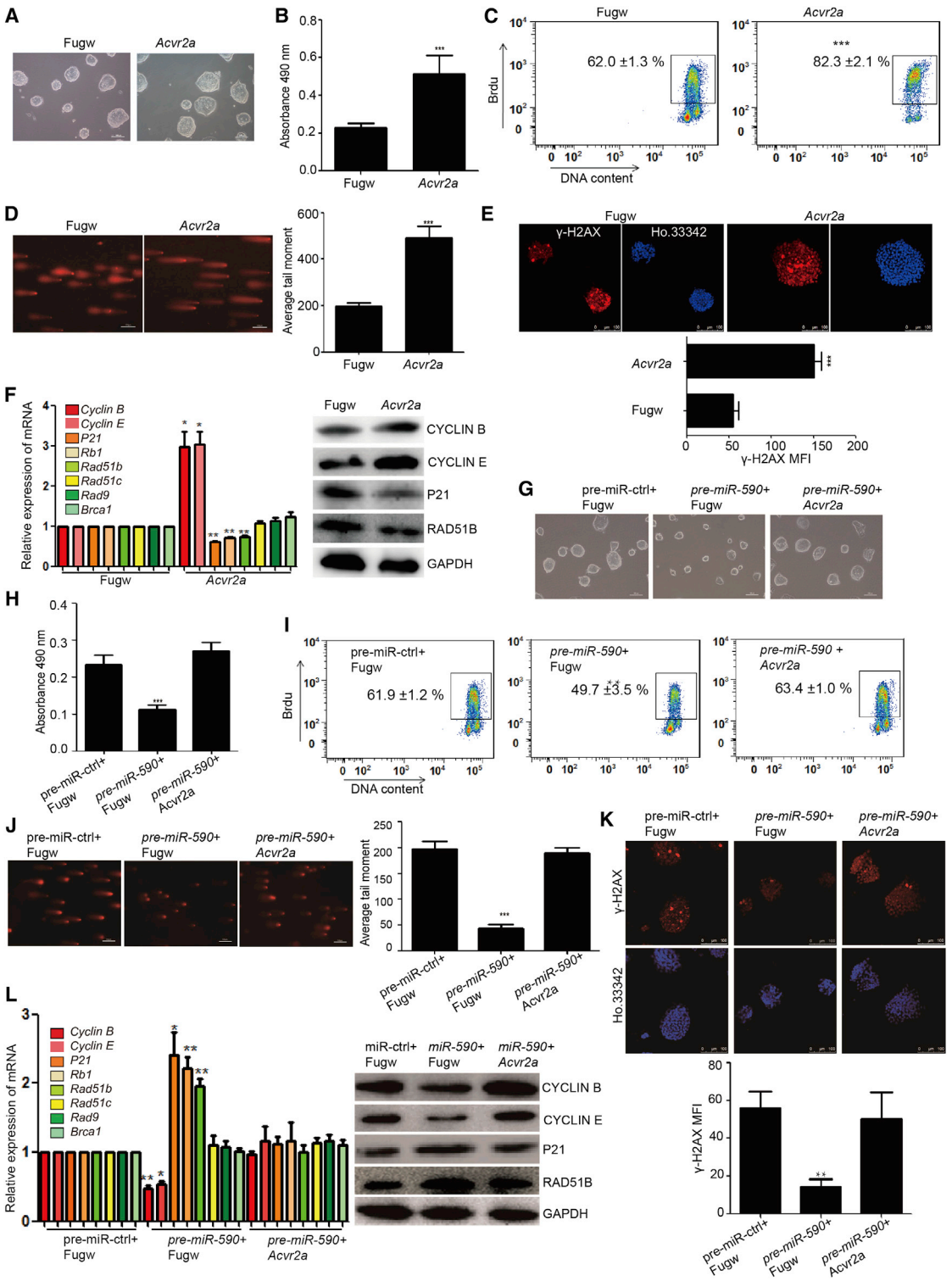

Figure 4. *miR-590* Regulates the SSB Damage Repair, DSB Damage Repair, and Proliferation of mESCs by *Acvr2a*

(A) Morphology of mESCs clones overexpressing *Acvr2a*. The scale bar represents 100 μm.

(B) Analysis of proliferation of mESCs overexpressed with *Acvr2a* by MTS cell proliferation assay. Data shown are means ± SD of five independent experiments (n = 5). ***p < 0.001.

(legend continued on next page)

collapsing during rapid and continuous proliferation in ESCs (Saretzki et al., 2004). We found that overexpression of *miR-590* significantly decreased DNA damage of mESCs by detecting the state of SSB and DSB damage. Our results suggested that *miR-590* might be the link between rapid proliferation and DNA damage repair in mESCs. Furthermore, we found that *miR-590* can accelerate the process of DNA damage repair after irradiation by X-ray but that *miR-590* does not weaken the radiation sensitivity. These results showed that *miR-590* not only influences the proliferation and cell cycle to assist the process of damage repair but also participates in DNA damage repair, especially for SSB and DSB repair.

Activin signaling has been reported to be crucial in maintaining ESC pluripotency and proliferation (Beattie et al., 2005; Ogawa et al., 2007). *Activin* performs its function through *Acvr2a*, which is required for binding *Activin* to cause downstream p-SMAD2 activation, thus initiating *Activin* signaling. *Activin* signaling has also been reported to participate in the DNA damage response. A study has also shown that *Activin* signaling potentiates epithelial support cell proliferation by *Acvr2a* and *Acvr2b*. Blocking *Activin-Acvr2a/b* signaling inhibits epithelial support cell proliferation, whereas an *Activin* receptor agonist increases proliferation (McCullar et al., 2010). Specific knockout of *Activin βA* in fetal Leydig cells represses sertoli cell proliferation (Archambeault and Yao, 2010). In our study, we found that the level of *Acvr2a* expression can mediate the strength of *Activin* signaling and regulate the efficiency of DSB damage repair, SSB damage repair, and cell proliferation in mESCs. Overexpression of *Acvr2a* reduced the repair of DNA damage and promoted the proliferation at a faster rate. Knockdown of *Acvr2a* resulted in the opposite phenomenon. We further found that the level of *Acvr2a* was higher in mESCs cultured in medium with LIF, which contrasted the expression of *miR-590*. More importantly, we determined that *Acvr2a* is the target gene of *miR-590* in mESCs. *miR-590* regulates the amount of *Acvr2a* on cell membranes to regulate *Activin* signaling in mESCs, thereby balancing mESC proliferation and DNA damage repair.

There are two major repair methods for DSB damage repair, namely HRR and nonhomologous end joining (NHEJ). HRR results in error-free repair, but NHEJ sometimes leads to errors. During HRR, DSB damage repair uses a template containing hundreds of base pairs of sequence homology, and usually the sister chromatids are available to serve as templates (Haber, 2000; Morrison et al., 2000; Takata et al., 1998). The S phase of ESCs has a long duration, so most of the ESC genomes would have sister chromatids, which assures the process of HHR (Tichy and Stambrook, 2008). *Rad51b* has been reported to play an important role in the HRR process to repair DSB, and *Rad51b* is also a protein kinase that can regulate cell cycle-related genes (Havre et al., 2000; Shrivastav et al., 2008; Stordal and Davey, 2009). In our study, we found that *Rad51b* is also important for mESCs. Knockdown of *Rad51b* results in inefficient DNA damage repair and a faster cell cycle, which creates a vicious circle of producing more DSB and SSB damage. We further found that Rad51B

(C) Analysis of proliferation of mESCs overexpressed with *Acvr2a* by FACS analysis of BrdU incorporation. The figure means the percentage of the population of BrdU-positive cells. Data shown are means ± SD of three independent experiments (n = 3). ***p < 0.001.
(D) Comet assay for SSB damage in mESCs. The scale bar represents 100 μm. Right panel is the quantification of average DNA tail moment. Data shown are means ± SD of three independent experiments (n = 3). ***p < 0.001.
(E) Immunofluorescence analysis of γ-H2AX (red) to indicate the state of DSB damage in mESCs. Ho.33342 (Hoechst 33342) represents nuclear staining (blue). The scale bar represents 100 μm. (Bottom) The quantification of the fluorescence of γ-H2AX immunostaining. Data shown are means ± SD of three independent experiments (n = 3). ***p < 0.001.
(F) qRT-PCR verification of transcript levels of the cell cycle regulation and homologous recombination damage repair genes in mESCs. The right side shows the protein levels according to western blot analysis. Data shown are means ± SD of three independent experiments (n = 3). *p < 0.05 and **p < 0.01.
(G) Morphology of mESCs clones. The scale bar represents 100 μm.
(H) Cell proliferation assay in the rescue experiment by MTS cell proliferation assay. Data shown are means ± SD of three independent experiments (n = 3). ***p < 0.001.
(I) Cell proliferation assay in the rescue experiment by FACS of BrdU incorporation. The figure means the percentage of the population of BrdU-positive cells. Data shown are means ± SD of three independent experiments (n = 3). **p < 0.01.
(J) Comet assay shows the SSB damage state. The scale bar represents 100 μm. The right panel is the quantification of average DNA tail moment. Data shown are means ± SD of three independent experiments (n = 3). ***p < 0.001.
(K) Overexpression of ACVR2a restores DSB damage in mESCs transfected with pre-*miR-590*. Immunofluorescence analysis of γ-H2AX (red) indicates the state of DSB damage in mESCs with Ho. 33342 (Hoechst 33342) staining for the nucleus (blue). The scale bar represents 100 μm. (Bottom) The quantification of the fluorescence of γ-H2AX immunostaining. Data shown are means ± SD of three independent experiments (n = 3). **p < 0.01.
(L) qRT-PCR and western blot analysis of the cell cycle- and homologous recombination damage repair-related genes in mESCs. Data shown are means ± SD of three independent experiments (n = 3). *p < 0.05 and **p < 0.01.

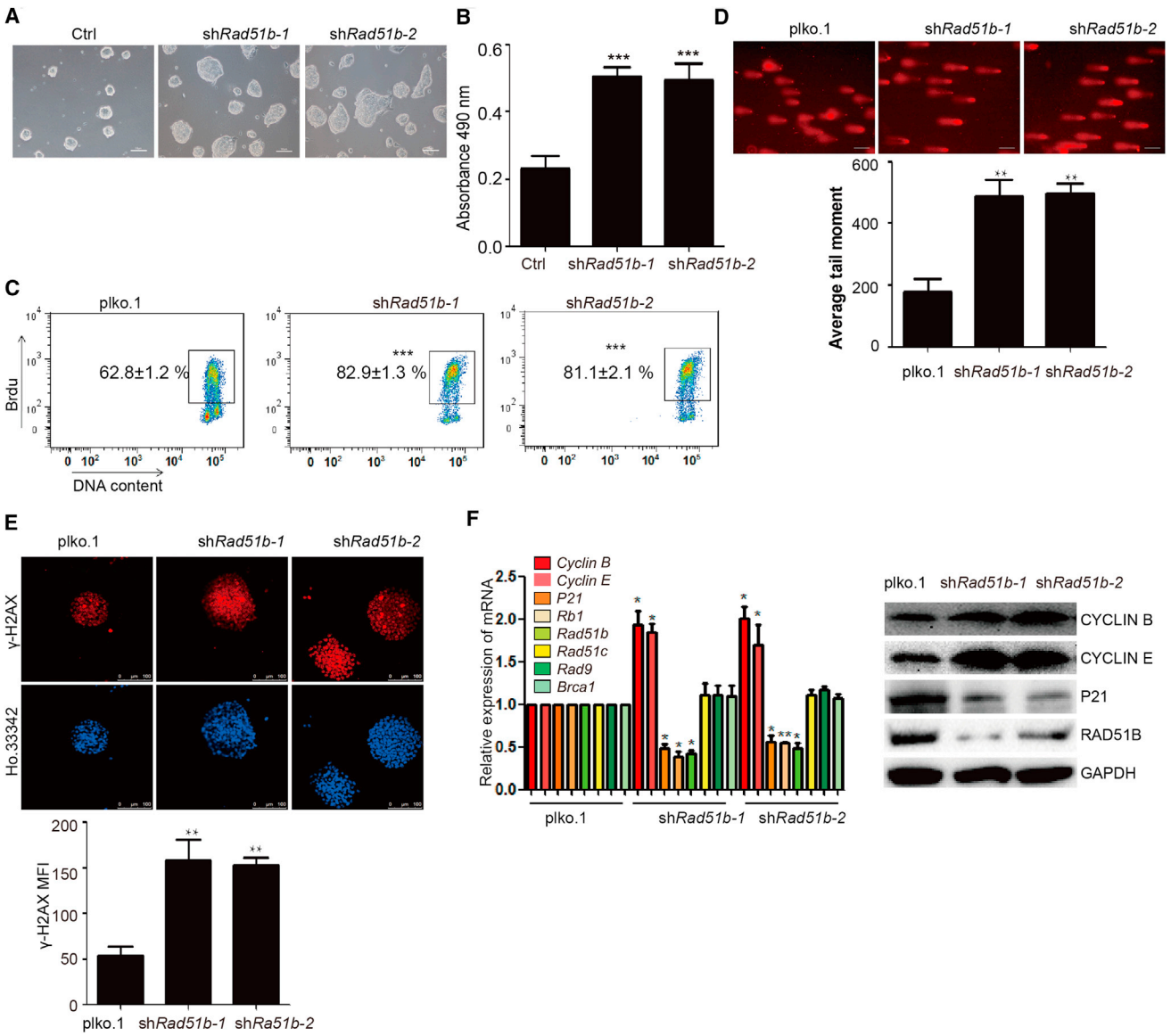

Figure 5. *Rad51b* Promotes SSB and DSB Damage Repair in mESCs and Slows the Cell Proliferation

(A) Morphology of mESC clones with knockdown of *Rad51b* compared with the control group. The scale bar represents 100 μm.

(B) Cell proliferation assay by MTS cell proliferation assay. Data shown are means ± SD of three independent experiments (n = 3). ***p < 0.001.

(C) Cell proliferation assay by FACS of BrdU incorporation. The figure means the percentage of the population of BrdU-positive cells in total cells. Figure shows the percentage of the population of BrdU-positive cells. Data shown are means ± SD of three independent experiments (n = 3). ***p < 0.001.

(D) Knockdown of *Rad51b* increases the SSB damage in mESCs as detected by the comet assay. The scale bar represents 100 μm. Bottom panel shows the quantification of average DNA tail moment. Data shown are means ± SD of three independent experiments (n = 3). **p < 0.01.

(E) Immunofluorescence analysis of γ-H2AX (red) indicates the state of DSB damage. γ-H2AX was increased by knockdown of *Rad51b* in mESCs. Ho.33342 (Hoechst 33342) represents nuclear staining (blue). The scale bar represents 100 μm. (Bottom) The quantification of the fluorescence of γ-H2AX immunostaining. Data shown are means ± SD of three independent experiments (n = 3). **p < 0.01.

(F) qRT-PCR and western blot indicating the levels of the cell cycle- and homologous recombination damage repair-related genes in mESCs. Data shown are means ± SD of three independent experiments (n = 3). *p < 0.05 and **p < 0.01.

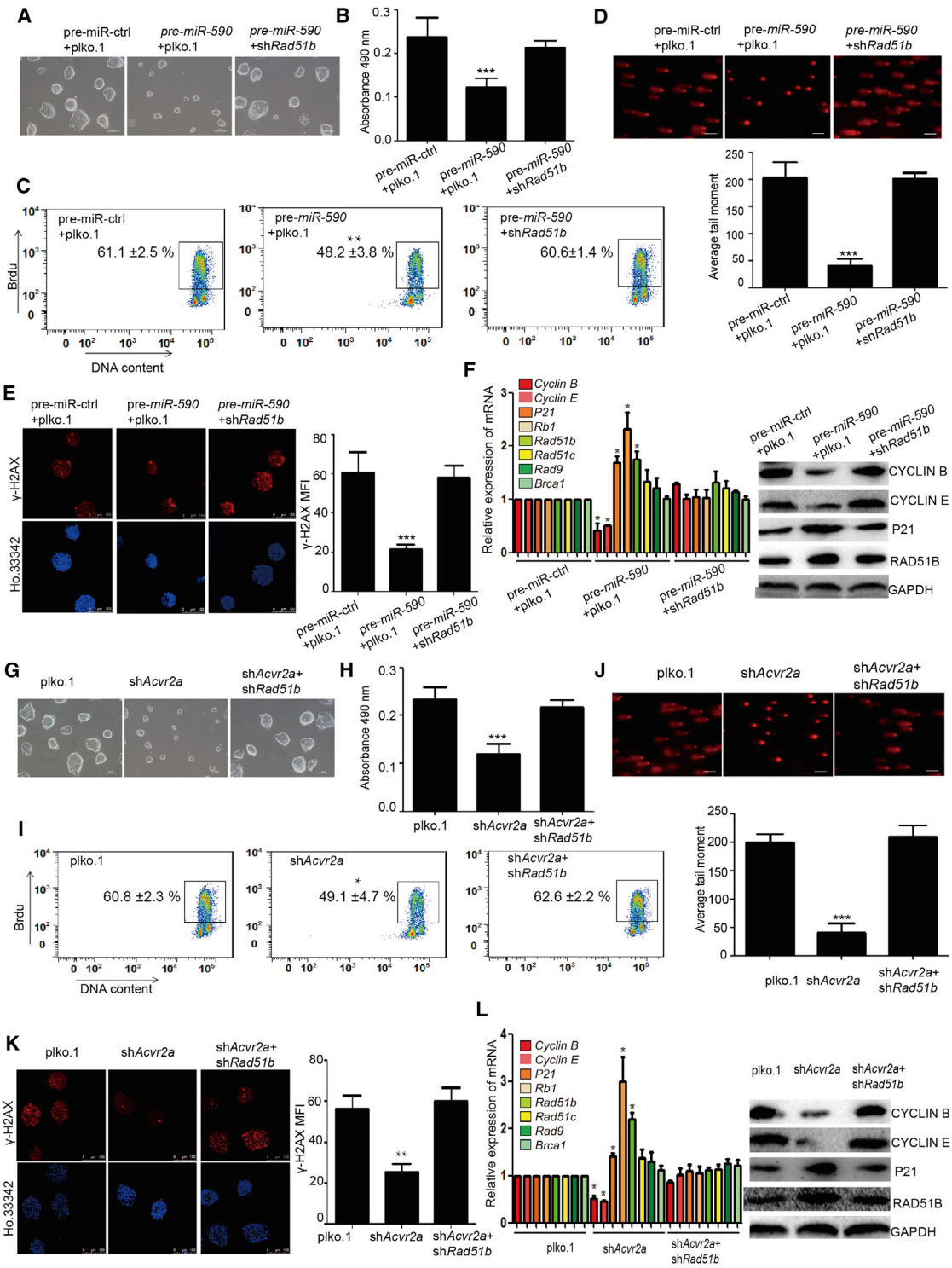

Figure 6. Knockdown of *Rad51b* Restores the State of Proliferation and DNA Damage in mESCs Overexpressing Pre-*miR-590* or Knockdown of *Acvr2a*

(A) Knockdown of *Rad51b* can restore the size of mESC clones influenced by *miR-590*. The scale bar represents 100 μm.

(B) Cell proliferation assay by MTS cell proliferation assay. Data shown are means ± SD of five independent experiments (n = 5). ***p < 0.001.

(legend continued on next page)

can be regulated by the *miR-590-Acvr2a* pathway. *Rad51b* can be upregulated by *miR-590* or knockdown of *Acvr2a* in mESCs. Moreover, knockdown of *Rad51b* attenuated the effects caused by knockdown of *Acvr2a* or overexpression of *miR-590*. Our results suggested that *miR-590/Acvr2a/Rad51b* signaling axis balances the coexistence of DNA damage repair and rapid proliferation, assuring the stabilization of mESCs. Our study provides insights into the regulation of proliferation and DNA damage repair during mESC self-renewal, and it suggests that an ESC-related signaling pathway not only maintains the stabilization of mESC self-renewal or pluripotency but also may be the regulator or responder of DNA damage repair.

EXPERIMENTAL PROCEDURES

mESC Culture

mESCs (E14) were cultured on feeder-free, gelatin-coated plates with Dulbecco's modified Eagle's medium (Hyclone) supplemented with LIF, 15% fetal bovine serum (GIBCO), 1% nonessential amino acids (Invitrogen, Life Technologies), 1% Gln (Invitrogen), and 0.18% β-mercaptoethanol (Sigma). mESCs were cultured at 37°C in a humidified 5% CO_2 atmosphere. 46C is another kind of mESC line that cultures in the same condition as E14.

Comet Assay

A comet assay was performed according to the comet assay kit (Cwbio).

All other methods can be found in the Supplemental Information.

SUPPLEMENTAL INFORMATION

Supplemental Information includes Supplemental Experimental Procedures and five figures and can be found with this article online at http://dx.doi.org/10.1016/j.stemcr.2014.10.006.

ACKNOWLEDGMENTS

This work was supported by grants obtained from the Ministry of Science and Technology (grant numbers 2011CB965100, 2013CB967600, 2011CBA01100, 2012CB966603, and 2013CB967401), the National Natural Science Foundation of China (grant numbers 91219305, 31210103905, 31371510, 31101061, 31171432, 81170499, 31201107, 31301208, and 81201599), the Science and Technology Commission of Shanghai Municipality (grant number 12ZR1450900), IRT1168 from Ministry of Education, sponsored by Shanghai Rising-Star Program (14QA1403900), the Specialized Research Fund for the Doctoral Program of Higher Education (20110072110039), support of the "Chen Guang" project from the Shanghai Municipal Education Commission and Shanghai Education Development Foundation (12CG19), and the Fundamental Research Funds for the Central Universities (2000219099).

Received: February 2, 2014
Revised: October 16, 2014
Accepted: October 16, 2014
Published: November 20, 2014

REFERENCES

Archambeault, D.R., and Yao, H.H. (2010). Activin A, a product of fetal Leydig cells, is a unique paracrine regulator of Sertoli cell

(C) Cell proliferation assay by FACS of BrdU incorporation. The figure means the percentage of the population of BrdU-positive cells. Figure shows the percentage of the population of BrdU-positive cells. Data shown are means ± SD of three independent experiments (n = 3). **p < 0.01.
(D) The comet assay shows that knockdown of *Rad51b* relieves the inhibition of SSB damage caused by *miR-590*. The scale bar represents 100 μm. (Bottom) The quantification of average DNA tail moment. Data shown are means ± SD of five independent experiments (n = 5). ***p < 0.001.
(E) Immunofluorescence analysis of γ-H2AX (red) to show DSB damage of mESCs. Nuclei were stained with Ho.33342 (Hoechst 33342) (blue). The scale bar represents 100 μm. The right panel shows the quantification of the fluorescence of γ-H2AX immunostaining. Data shown are means ± SD of three independent experiments (n = 3). ***p < 0.001.
(F) qRT-PCR indicated that the levels of the cell cycle- and homologous recombination damage repair-related genes were rescued by downregulating *Rad51b* in mESCs transfected with pre-*miR-590*. The right side shows the protein levels detected by western blot analysis. *p < 0.05 and **p < 0.01.
(G) Knockdown of *Rad51b* restores the size mESC clones containing knockdown of *Acvr2a*. The scale bar represents 100 μm.
(H) MTS cell proliferation assay. Data shown are means ± SD of five independent experiments (n = 5). ***p < 0.001.
(I) FACS analysis of BrdU incorporation. The figure means the percentage of the population of BrdU-positive cells. Figure shows the percentage of the population of BrdU-positive cells. Data shown are means ± SD of three independent experiments (n = 3). *p < 0.05.
(J) The comet assay. The scale bar represents 100 μm. (Bottom) The quantification of average DNA tail moment. Data shown are means ± SD of three independent experiments (n = 3). ***p < 0.001.
(K) Immunofluorescence analysis of γ-H2AX (red). Nuclei were stained with Ho.33342 (Hoechst 33342) (blue). The scale bar represents 100 μm. The right panel shows the quantification of the fluorescence of γ-H2AX immunostaining. Data shown are means ± SD of three independent experiments (n = 3). **p < 0.01.
(L) qRT-PCR of the cell cycle- and homologous recombination damage repair-related genes in mESCs. The right side shows the protein levels as detected by western blot analysis. Data shown are means ± SD of three independent experiments (n = 3). *p < 0.05.

proliferation and fetal testis cord expansion. Proc. Natl. Acad. Sci. USA *107*, 10526–10531.

Banáth, J.P., Bañuelos, C.A., Klokov, D., MacPhail, S.M., Lansdorp, P.M., and Olive, P.L. (2009). Explanation for excessive DNA single-strand breaks and endogenous repair foci in pluripotent mouse embryonic stem cells. Exp. Cell Res. *315*, 1505–1520.

Baumann, P., Benson, F.E., and West, S.C. (1996). Human Rad51 protein promotes ATP-dependent homologous pairing and strand transfer reactions in vitro. Cell *87*, 757–766.

Beattie, G.M., Lopez, A.D., Bucay, N., Hinton, A., Firpo, M.T., King, C.C., and Hayek, A. (2005). Activin A maintains pluripotency of human embryonic stem cells in the absence of feeder layers. Stem Cells *23*, 489–495.

Bondestam, J., Horelli-Kuitunen, N., Hildén, K., Ritvos, O., and Aaltonen, J. (1999). Assignment of ACVR2 and ACVR2B the human activin receptor type II and IIB genes to chromosome bands 2q22.2—>q23.3 and 3p22 and the human follistatin gene (FST) to chromosome 5q11.2 by FISH. Cytogenet. Cell Genet. *87*, 219–220.

Carlson, B.C., Hofer, M.D., Ballek, N., Yang, X.J., Meeks, J.J., and Gonzalez, C.M. (2013). Protein markers of malignant potential in penile and vulvar lichen sclerosus. J. Urol. *190*, 399–406.

Chen, K., and Rajewsky, N. (2007). The evolution of gene regulation by transcription factors and microRNAs. Nat. Rev. Genet. *8*, 93–103.

Chun, J., Buechelmaier, E.S., and Powell, S.N. (2013). Rad51 paralog complexes BCDX2 and CX3 act at different stages in the BRCA1-BRCA2-dependent homologous recombination pathway. Mol. Cell. Biol. *33*, 387–395.

Chuykin, I.A., Lianguzova, M.S., Pospelova, T.V., and Pospelov, V.A. (2008). Activation of DNA damage response signaling in mouse embryonic stem cells. Cell Cycle *7*, 2922–2928.

Donaldson, C.J., Mathews, L.S., and Vale, W.W. (1992). Molecular cloning and binding properties of the human type II activin receptor. Biochem. Biophys. Res. Commun. *184*, 310–316.

Donoho, G., Jasin, M., and Berg, P. (1998). Analysis of gene targeting and intrachromosomal homologous recombination stimulated by genomic double-strand breaks in mouse embryonic stem cells. Mol. Cell. Biol. *18*, 4070–4078.

Dubrovska, A., Kanamoto, T., Lomnytska, M., Heldin, C.H., Volodko, N., and Souchelnytskyi, S. (2005). TGFbeta1/Smad3 counteracts BRCA1-dependent repair of DNA damage. Oncogene *24*, 2289–2297.

Favreau, A.J., and Sathyanarayana, P. (2012). miR-590-5p, miR-219-5p, miR-15b and miR-628-5p are commonly regulated by IL-3, GM-CSF and G-CSF in acute myeloid leukemia. Leuk. Res. *36*, 334–341.

Fluckiger, A.C., Marcy, G., Marchand, M., Négre, D., Cosset, F.L., Mitalipov, S., Wolf, D., Savatier, P., and Dehay, C. (2006). Cell cycle features of primate embryonic stem cells. Stem Cells *24*, 547–556.

Fordyce, C.A., Patten, K.T., Fessenden, T.B., DeFilippis, R., Hwang, E.S., Zhao, J., and Tlsty, T.D. (2012). Cell-extrinsic consequences of epithelial stress: activation of protumorigenic tissue phenotypes. Breast Cancer Res. *14*, R155.

Furue, M., Okamoto, T., Hayashi, Y., Okochi, H., Fujimoto, M., Myoishi, Y., Abe, T., Ohnuma, K., Sato, G.H., Asashima, M., and Sato, J.D. (2005). Leukemia inhibitory factor as an anti-apoptotic mitogen for pluripotent mouse embryonic stem cells in a serum-free medium without feeder cells. In Vitro Cell. Dev. Biol. Anim. *41*, 19–28.

Haber, J.E. (2000). Partners and pathwaysrepairing a double-strand break. Trends Genet. *16*, 259–264.

Hasty, P., Rivera-Pérez, J., and Bradley, A. (1992). The role and fate of DNA ends for homologous recombination in embryonic stem cells. Mol. Cell. Biol. *12*, 2464–2474.

Havre, P.A., Rice, M.C., Noe, M., and Kmiec, E.B. (1998). The human REC2/RAD51B gene acts as a DNA damage sensor by inducing G1 delay and hypersensitivity to ultraviolet irradiation. Cancer Res. *58*, 4733–4739.

Havre, P.A., Rice, M., Ramos, R., and Kmiec, E.B. (2000). HsRec2/Rad51L1, a protein influencing cell cycle progression, has protein kinase activity. Exp. Cell Res. *254*, 33–44.

Hong, Y., and Stambrook, P.J. (2004). Restoration of an absent G1 arrest and protection from apoptosis in embryonic stem cells after ionizing radiation. Proc. Natl. Acad. Sci. USA *101*, 14443–14448.

Ishikawa, K., Ishii, H., and Saito, T. (2006). DNA damage-dependent cell cycle checkpoints and genomic stability. DNA Cell Biol. *25*, 406–411.

Jensen, R.B., Carreira, A., and Kowalczykowski, S.C. (2010). Purified human BRCA2 stimulates RAD51-mediated recombination. Nature *467*, 678–683.

Jensen, R.B., Ozes, A., Kim, T., Estep, A., and Kowalczykowski, S.C. (2013). BRCA2 is epistatic to the RAD51 paralogs in response to DNA damage. DNA Repair (Amst.) *12*, 306–311.

Kanamoto, T., Hellman, U., Heldin, C.H., and Souchelnytskyi, S. (2002). Functional proteomics of transforming growth factor-beta1-stimulated Mv1Lu epithelial cells: Rad51 as a target of TGFbeta1-dependent regulation of DNA repair. EMBO J. *21*, 1219–1230.

Kawabata, M., Kawabata, T., and Nishibori, M. (2005). Role of recA/RAD51 family proteins in mammals. Acta Med. Okayama *59*, 1–9.

Keller, G. (2005). Embryonic stem cell differentiation: emergence of a new era in biology and medicine. Genes Dev. *19*, 1129–1155.

Lal, A., Pan, Y., Navarro, F., Dykxhoorn, D.M., Moreau, L., Meire, E., Bentwich, Z., Lieberman, J., and Chowdhury, D. (2009). miR-24-mediated downregulation of H2AX suppresses DNA repair in terminally differentiated blood cells. Nat. Struct. Mol. Biol. *16*, 492–498.

Li, V.C., Ballabeni, A., and Kirschner, M.W. (2012). Gap 1 phase length and mouse embryonic stem cell self-renewal. Proc. Natl. Acad. Sci. USA *109*, 12550–12555.

Lipchina, I., Elkabetz, Y., Hafner, M., Sheridan, R., Mihailovic, A., Tuschl, T., Sander, C., Studer, L., and Betel, D. (2011). Genome-wide identification of microRNA targets in human ES cells reveals a role for miR-302 in modulating BMP response. Genes Dev. *25*, 2173–2186.

Marson, A., Levine, S.S., Cole, M.F., Frampton, G.M., Brambrink, T., Johnstone, S., Guenther, M.G., Johnston, W.K., Wernig, M., Newman, J., et al. (2008). Connecting microRNA genes to the core

transcriptional regulatory circuitry of embryonic stem cells. Cell *134*, 521–533.

McCullar, J.S., Ty, S., Campbell, S., and Oesterle, E.C. (2010). Activin potentiates proliferation in mature avian auditory sensory epithelium. J. Neurosci. *30*, 478–490.

Mitra, D., Fernandez, P., Bian, L., Song, N., Li, F., Han, G., and Wang, X.J. (2013). Smad4 loss in mouse keratinocytes leads to increased susceptibility to UV carcinogenesis with reduced Ercc1-mediated DNA repair. J. Invest. Dermatol. *133*, 2609–2616.

Mo, M., Peng, F., Wang, L., Peng, L., Lan, G., and Yu, S. (2013). Roles of mitochondrial transcription factor A and microRNA-590-3p in the development of bladder cancer. Oncol. Lett. *6*, 617–623.

Momcilovic, O., Knobloch, L., Fornsaglio, J., Varum, S., Easley, C., and Schatten, G. (2010). DNA damage responses in human induced pluripotent stem cells and embryonic stem cells. PLoS ONE *5*, e13410.

Morrison, C., Sonoda, E., Takao, N., Shinohara, A., Yamamoto, K., and Takeda, S. (2000). The controlling role of ATM in homologous recombinational repair of DNA damage. EMBO J. *19*, 463–471.

Moskwa, P., Buffa, F.M., Pan, Y., Panchakshari, R., Gottipati, P., Muschel, R.J., Beech, J., Kulshrestha, R., Abdelmohsen, K., Weinstock, D.M., et al. (2011). miR-182-mediated downregulation of BRCA1 impacts DNA repair and sensitivity to PARP inhibitors. Mol. Cell *41*, 210–220.

Ogawa, K., Saito, A., Matsui, H., Suzuki, H., Ohtsuka, S., Shimosato, D., Morishita, Y., Watabe, T., Niwa, H., and Miyazono, K. (2007). Activin-Nodal signaling is involved in propagation of mouse embryonic stem cells. J. Cell Sci. *120*, 55–65.

Pothof, J., Verkaik, N.S., van IJcken, W., Wiemer, E.A., Ta, V.T., van der Horst, G.T., Jaspers, N.G., van Gent, D.C., Hoeijmakers, J.H., and Persengiev, S.P. (2009). MicroRNA-mediated gene silencing modulates the UV-induced DNA-damage response. EMBO J. *28*, 2090–2099.

Qi, X., Li, T.G., Hao, J., Hu, J., Wang, J., Simmons, H., Miura, S., Mishina, Y., and Zhao, G.Q. (2004). BMP4 supports self-renewal of embryonic stem cells by inhibiting mitogen-activated protein kinase pathways. Proc. Natl. Acad. Sci. USA *101*, 6027–6032.

Robson, N.C., Phillips, D.J., McAlpine, T., Shin, A., Svobodova, S., Toy, T., Pillay, V., Kirkpatrick, N., Zanker, D., Wilson, K., et al. (2008). Activin-A: a novel dendritic cell-derived cytokine that potently attenuates CD40 ligand-specific cytokine and chemokine production. Blood *111*, 2733–2743.

Ruiz, S., Panopoulos, A.D., Herrerías, A., Bissig, K.D., Lutz, M., Berggren, W.T., Verma, I.M., and Izpisua Belmonte, J.C. (2011). A high proliferation rate is required for cell reprogramming and maintenance of human embryonic stem cell identity. Curr. Biol. *21*, 45–52.

Saretzki, G., Armstrong, L., Leake, A., Lako, M., and von Zglinicki, T. (2004). Stress defense in murine embryonic stem cells is superior to that of various differentiated murine cells. Stem Cells *22*, 962–971.

Savatier, P., Lapillonne, H., Jirmanova, L., Vitelli, L., and Samarut, J. (2002). Analysis of the cell cycle in mouse embryonic stem cells. Methods Mol. Biol. *185*, 27–33.

Shrivastav, M., De Haro, L.P., and Nickoloff, J.A. (2008). Regulation of DNA double-strand break repair pathway choice. Cell Res. *18*, 134–147.

Smih, F., Rouet, P., Romanienko, P.J., and Jasin, M. (1995). Double-strand breaks at the target locus stimulate gene targeting in embryonic stem cells. Nucleic Acids Res. *23*, 5012–5019.

Song, L., Lin, C., Wu, Z., Gong, H., Zeng, Y., Wu, J., Li, M., and Li, J. (2011). miR-18a impairs DNA damage response through downregulation of ataxia telangiectasia mutated (ATM) kinase. PLoS ONE *6*, e25454.

Stordal, B., and Davey, R. (2009). ERCC1 expression and RAD51B activity correlate with cell cycle response to platinum drug treatment not DNA repair. Cancer Chemother. Pharmacol. *63*, 661–672.

Strumberg, D., Pilon, A.A., Smith, M., Hickey, R., Malkas, L., and Pommier, Y. (2000). Conversion of topoisomerase I cleavage complexes on the leading strand of ribosomal DNA into 5′-phosphorylated DNA double-strand breaks by replication runoff. Mol. Cell. Biol. *20*, 3977–3987.

Takata, M., Sasaki, M.S., Sonoda, E., Morrison, C., Hashimoto, M., Utsumi, H., Yamaguchi-Iwai, Y., Shinohara, A., and Takeda, S. (1998). Homologous recombination and non-homologous end-joining pathways of DNA double-strand break repair have overlapping roles in the maintenance of chromosomal integrity in vertebrate cells. EMBO J. *17*, 5497–5508.

Takata, M., Sasaki, M.S., Sonoda, E., Fukushima, T., Morrison, C., Albala, J.S., Swagemakers, S.M., Kanaar, R., Thompson, L.H., and Takeda, S. (2000). The Rad51 paralog Rad51B promotes homologous recombinational repair. Mol. Cell. Biol. *20*, 6476–6482.

Thacker, J. (2005). The RAD51 gene family, genetic instability and cancer. Cancer Lett. *219*, 125–135.

Tichy, E.D. (2011). Mechanisms maintaining genomic integrity in embryonic stem cells and induced pluripotent stem cells. Exp. Biol. Med. (Maywood) *236*, 987–996.

Tichy, E.D., and Stambrook, P.J. (2008). DNA repair in murine embryonic stem cells and differentiated cells. Exp. Cell Res. *314*, 1929–1936.

Tichy, E.D., Pillai, R., Deng, L., Liang, L., Tischfield, J., Schwemberger, S.J., Babcock, G.F., and Stambrook, P.J. (2010). Mouse embryonic stem cells, but not somatic cells, predominantly use homologous recombination to repair double-strand DNA breaks. Stem Cells Dev. *19*, 1699–1711.

Turinetto, V., Orlando, L., Sanchez-Ripoll, Y., Kumpfmueller, B., Storm, M.P., Porcedda, P., Minieri, V., Saviozzi, S., Accomasso, L., Cibrario Rocchietti, E., et al. (2012). High basal γH2AX levels sustain self-renewal of mouse embryonic and induced pluripotent stem cells. Stem Cells *30*, 1414–1423.

Valerie, K., and Povirk, L.F. (2003). Regulation and mechanisms of mammalian double-strand break repair. Oncogene *22*, 5792–5812.

Villa, C., Fenoglio, C., De Riz, M., Clerici, F., Marcone, A., Benussi, L., Ghidoni, R., Gallone, S., Cortini, F., Serpente, M., et al. (2011). Role of hnRNP-A1 and miR-590-3p in neuronal

death: genetics and expression analysis in patients with Alzheimer disease and frontotemporal lobar degeneration. Rejuvenation Res. *14*, 275–281.

Wan, G., Mathur, R., Hu, X., Zhang, X., and Lu, X. (2011). miRNA response to DNA damage. Trends Biochem. Sci. *36*, 478–484.

Wang, Y., Baskerville, S., Shenoy, A., Babiarz, J.E., Baehner, L., and Blelloch, R. (2008). Embryonic stem cell-specific microRNAs regulate the G1-S transition and promote rapid proliferation. Nat. Genet. *40*, 1478–1483.

White, J., and Dalton, S. (2005). Cell cycle control of embryonic stem cells. Stem Cell Rev. *1*, 131–138.

Stem Cell Reports, Volume *3*

Supplemental Information

A *miR-590/Acvr2a/Rad51b* Axis Regulates DNA Damage Repair during mESC Proliferation

Qidong Liu, Guiying Wang, Yafang Chen, Guoping Li, Dandan Yang, and Jiuhong Kang

Supplementary Information

I. Supplemental Experimental Procedures

Western blot

Cells were lysed with 1×loading lysis buffer that was diluted from 5×loading lysis buffer (2.5 ml of 0.5 mol/L Tris-HCl at pH 6.8 containing 0.39 g of DTT, 0.5 g of SDS, and 0.025 g of bromophenol blue added to 2.5 ml of glycerine). Equal amount of protein was transferred onto PVDF membranes (BioRad, USA). Protein was detected by primary antibodies against CYCLIN B (sc-752, Santa Cruz, California, USA), P21 (sc-6246, Santa Cruz), CYCLIN E (sc-481, Santa Cruz), GAPDH (sc-47724, Santa Cruz), RAD51B (BS2542, Bioworld, Nanjing, China), p-SMAD2 (BS4172, Bioworld), ACVR2A (BS3669, Bioworld), and SMAD2/3 (BS1838, Bioworld).

Immunostaining

mES cells were fixed for 20 min in 4% paraformaldehyde. The cells were then washed 3 times with PBS followed by treatment with 0.2% Triton X-100 for 7 min. The cells were then washed 3 times with PBS followed by treatment with PBS containing 10% FBS (Gibico) for 1 h at room temperature. The primary antibody was diluted in PBS containing 10% FBS and added to the cells for an overnight incubation at 4°C. The cells were then washed 3 times with PBS, and the secondary antibody was added to the cells for incubation at room temperature for 2 h. The primary antibody used for immunostaining was γ-H2AX (#2577, Cell Signaling Technology, Boston,

USA).

Quantification of fluorescence of γ-H2AX immunostaining and DNA tail comet assay

To quantify the fluorescence degree of γ-H2AX staining of each experiment, mES cell clones areas that should contains more than a hundred cells were selected. Fifty clones were selected in each group to detect the mean fluorescence intensity (MFI) that was expressed as arbitrary units per pixel by using LSM Image Examiner software. The comet assay software project (CASP) was used to analyze the DNA tail of comet assay.

Quantitative real-time PCR (qRT-PCR)

For miRNA

The total RNA was isolated using RNAiso (Takara, Japan). miRNA was subsequently reverse-transcribed to cDNA using the miRNA specific stem-loop reverse-transcription primer (Ribobio, China). The amount of target gene expression ($2^{-\Delta\Delta Ct}$) was normalized via the endogenous small nuclear RNA U6 using miRNA-specific primers (Ribobio). The reaction conditions were performed according to the instructions from Ribobio Co., Ltd with SYBR Green qPCR Mix (BioRad).

For mRNA

The total RNA was isolated using RNAiso (Takara). cDNA was subsequently

reverse-transcribed from mRNA by M-MLV Reverse Transcriptase (Takara). The PCR included 40 cycles of amplification using the Stratagene Mx3000P system with SYBR Green qPCR Mix (BioRad). Expression of target genes ($2^{-\Delta\Delta Ct}$) was normalized against *Gapdh*. The primers are shown below:

P21 (forward, 5'-CGAGAACGGTGGAACTTTGAC-3'; reverse, 5'-CAGGGCTCAGGTAGACCTTG-3')

Cyclin E (forward, 5'-GTGGCTCCGACCTTTCAGTC-3'; reverse, 5'-CACAGTCTTGTCAATCTTGGCA-3')

Cyclin B (forward, 5'- AAGGTGCCTGTGTGTGAACC-3'; reverse, 5'-GTCAGCCCCATCATCTGCG-3')

Rb1 (forward, 5'-TCCACCAGGCCTCCTACCT-3'; reverse, 5'-CCAGGAATCCGTAAGGGTGAA-3')

Acvr2a (forward, 5'-GCGTTCGCCGTCTTTCTTATC-3'; reverse, 5'-GTTGGTTCTGTCTCTTTCCCAAT-3')

Rad51b (forward, 5'-TGACGAATCAAATTACGACCCAT-3'; reverse, 5'-CCTAGTGCAGCTACCAAACAG-3')

Rad9 (forward, 5'- GGCTGTCCATTCGCTATCCC-3'; reverse, 5'-GTGGGGCAAAAAGGAAGCAG-3')

Rad51c (forward, 5'- CAACTGCCTGCATTCAGCAC-3'; reverse, 5'-TGCCAGCAGCTCAGTATAATCA-3')

Brca1 (forward, 5’-AGCCCACCTACTTGTGCTGA-3’; reverse, 5’-TCGATGAGTTGAGGCTCTCTAA-3’)

Oct4 (forward, 5’-GGATGCTGTGAGCCAAGG-3’; reverse, 5’-GAACAAAATGATGAGTGACAGACAG-3’)

Nanog (forward, 5’-CAGGTGTTTGAGGGTAGCTC-3’; reverse, 5’-CGGTTCATCATGGTACAGTC-3’)

Sox2 (forward, 5’-GATCAGCATGTACCTCCCC-3’; reverse, 5’- CCCTCCCAATTCCCTTGTATC -3’)

Gapdh (forward, 5’-GTGTTCCTACCCCCAATGTGT-3’; reverse, 5’-ATTGTCATACCAGGAAATGAGCTT-3’)

Trypan blue staining

Prepare 0.5 ml single cell suspension in PBS, and then add 0.5 ml trypan blue solution (0.4%) (Sigma). Allow to react for 3 min, and then calculate the total viable cells (unstained) and total cells (stained and unstained) by microscope to determine the cell viability. Cell viability (%) = viable cells / total cells ×100%.

Cell apoptosis analysis

Cell apoptosis analysis was performed by using AnnexinV-FITC Cell Apoptosis Detection kit (Keygentec, China).

mES cultured without LIF

The cells were cultured in the DMEM medium (Hyclone) supplemented with 15% FBS (Gibco), 1% NEAA (Invitrogen), 1% Gln (Invitrogen), without LIF and β-mercaptoethanol.

Embryonic bodies (EBs) formation

Single mES cell suspension was transferred into the bacteriologic dishes and cultured in the medium which is the same as the culture mentioned above.

Construction of vector

Luciferase reporter vector

3'UTR sequences of *Acvr2a* were amplified by PCR from mES cell genomic DNA and inserted into the pGL3-luciferase reporter gene vector. The mutant miRNA binding sites were obtained by replacing the miRNA binding site sequence with miRNA seed sequences using the QuickChange Lightning Multi Site-Directed Mutagenesis Kit (Agilent Technologies, USA).

Acvr2a overexpression vector

Fragment of mouse *Acvr2a* was cloned from the pCDNA-*Acvr2a* (Sino Biological, China) by the primers with the restriction enzyme cutting site of BamHI and EcoRI (forward, 5'-GGCCGGCCGATGGGAGCTGCTGCAAAGTT-3'; reverse, 5'-GGCGAATTCTCATAGACTAGATTCTTTGGGAGGA-3') and was inserted into Fugw vector.

Acvr2a-flag overexpression vector:

Fragment of mouse *Acvr2a*-flag was cloned from the pCDNA-*Acvr2a* by the primers with the restriction enzyme cutting site of BamHI and EcoRI (forward, 5'-GGCGGATCCATGGACTACAAGGACGACGATGACAAGGGAGCTGCTGCA AAGT-3'; reverse, 5'-GGCGAATTCTCATAGACTAGATTCTTTGGGAGGA-3) and inserted into Fugw vector.

Acvr2a and Rad51b knockdown vector:

The corresponding base pairs for sh*Acvr2a*- or sh*Rad51b*-specific regions (sh*Acvr2a*-1, CCTGTGGCTAATCACAGCATT; sh*Acvr2a*-2: GGTGTTGGA GGGTGCTATAAA; sh*Rad51b*-1: GCTGAGAGACTGGTTGAGATT; sh*Rad51b*-2: TGTTGACTCCATTGCTTCTGTGGTCAGAA) for RNA interference were designed and cloned into the pLKO.1-TRC cloning vector.

Luciferase assay

NIH3T3 cells (1×10^5 cells per well of 24-well plate) were transfected with 250 ng of luciferase reporter, 5 ng of Renilla vector (Promega), and 50 nM chemically synthesized *pre-miR-590* or pre-miRNA control (Biolend, China) using Fugene HD transfection reagent (Roche, Switzerland). Cell lysates were harvested at 24 h after transfection and subjected to the dual luciferase assay (Promega).

Transfection of pre-miRNA, miRNA mimics and inhibitors

The miRNA mimics (Ribobio) were artificially synthesized short double-stranded oligonucleotides, which can be processed by cells to produce mature miRNA. The miRNA inhibitors (Ribobio) were also artificially synthesized

single-stranded RNAs, which are the antisense oligonucleotides of mature miRNAs. miRNA inhibitors compete with the miRNAs for target mRNAs to inhibit the function of miRNAs. The pre-miRNA was an artificially synthesized oligonucleotide that was longer than the miRNA mimics. The synthesized pre-miRNA sequence was the same as the endogenous pre-miRNA sequence. The pre-miRNA, miRNA mimics and inhibitors were all transfected into cells using the Fugene HD transfection reagent (Roche).

Cell proliferation analysis

Cell proliferation analysis was performed by two different kinds of methods. One is MTS assay that was performed by using CellTiter 96® AQueous One Solution Cell Proliferation Assay kit (Promega, USA) which needs to detect the absorption value at 490 nm by using microplate reader.

Another is flow cytometric analysis of 5'-bromo-deoxyuridine (BrdU) incorporation. Cells were exposed to BrdU for 1 h before analyzing the proliferative activity. The BrdU incorporation into mES cells was quantified by BrdU Cell Proliferation Detection kit (Keygentec, China).

Statistical analyses

Student's *t*-test was used for all statistical analyses. Statistical significance was defined as follows: * means $p < 0.05$; ** means $p < 0.01$; and ***means $p < 0.001$. Values were presented as the mean ± SD.

II. Supplemental Figures and Figure Legends

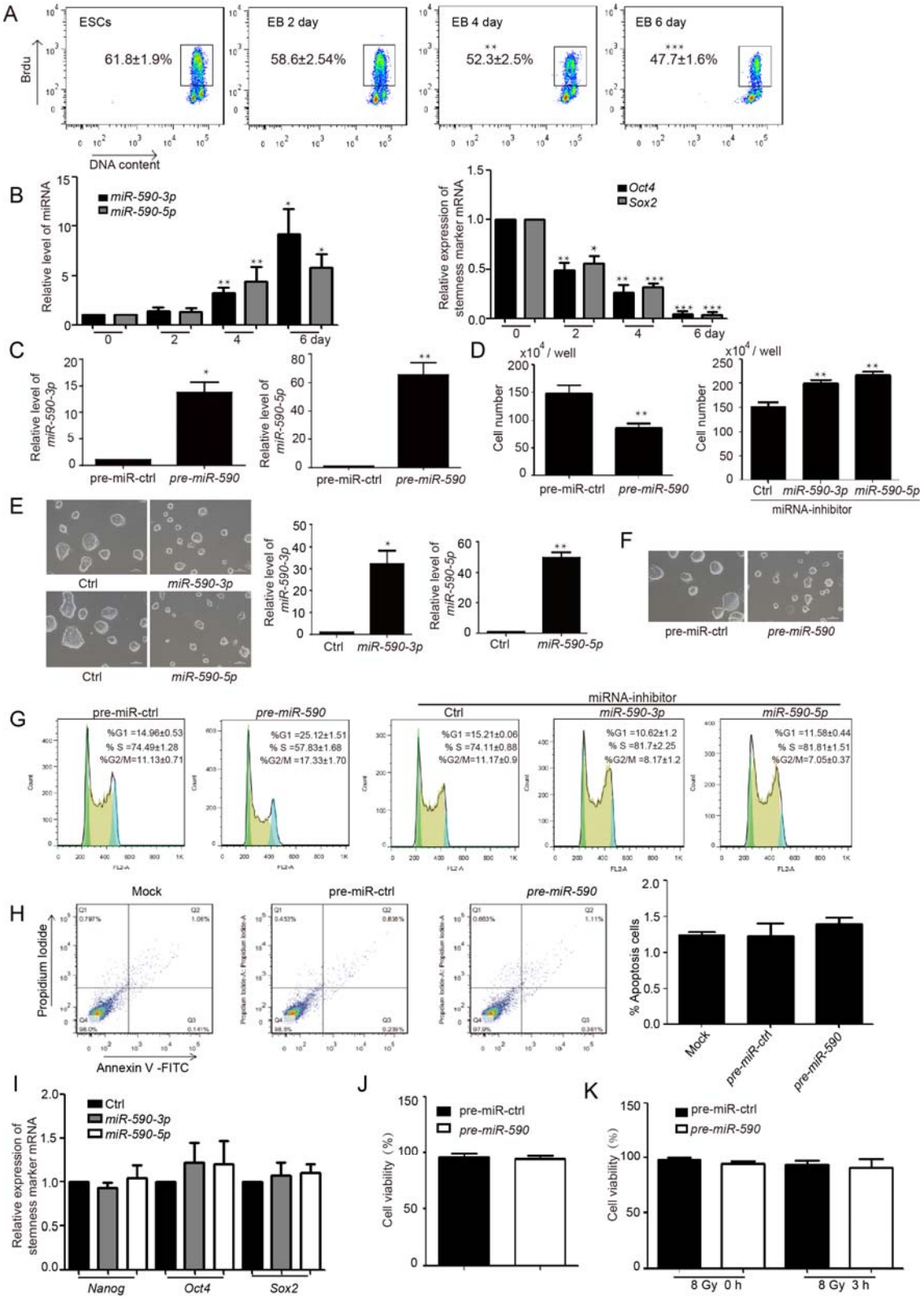

Figure S1

Figure S1, related to Figure 1. *miR-590-3p* and *miR-590-5p* can regulate the proliferation without influencing the stemness maintenance, cell apoptosis and death

(A) Analysis of the proliferation during EBs formation at d2, d4, d6 by FACS analysis of BrdU incorporation. Cells at d0 were mES cells. The figure showed the percentage (%) of population of BrdU positive cells. Data shown are means ± SD of three independent experiments (n=3). **p < 0.01 and ***p < 0.001.

(B) Level of *miR-590-3p/5p* detected by qRT-PCR during EBs formation (left panel). Right panel means detection of level of stemness markers (*Oct4, Sox2*) during EBs formation (right panel). Data shown are means ± SD of three independent experiments (n=3). *p < 0.05, **p < 0.01, and ***p < 0.001.

(C) Detection of *miR-590-3p* and *miR-590-5p* in mES cells transfected with pre-miR-590. Data shown are means ± SD of three independent experiments (n=3). *p < 0.05 and **p < 0.01.

(D) Counting of amount of the total cells of mES cells transfected with *pre-miR-590* or miRNA inhibitors. Data shown are means ± SD of three independent experiments (n=3). **p < 0.01.

(E) Morphology of mES cell clones transfected with *miR-590-3p* or *miR-590-5p* mimics respectively. The scale bar represents 100 μm. Right panel showed the expression level of *miR-590-3p* and *miR-590-5p* in mES cells transfected with *miR-590-3p* or *miR-590-5p* mimics respectively. Data shown are means ± SD of three

independent experiments (n=3). *p < 0.05 and **p < 0.01.

(F) Another kind of mES cells line (46C), transfected with *pre-miR-590* showed smaller clone than control. The scale bar represents 100 μm.

(G) Cell cycle analysis by flow cytometry after propidium iodide (PI) staining. Data shown are means ± SD of three independent experiments (n=3).

(H) Cell apoptosis analysis of mES cells transfected with *pre-miR-590*. Right panel showed the statistical analysis of the percentage of apoptosis cells. Data shown are means ± SD of three independent experiments (n=3).

(I) *miR-590-3p* and *miR-590-5p* cannot influence the stemness by detecting the stemness markers of *Nanog*, *Oct4*, and *Sox2* through qRT-PCR. Data shown are means ± SD of three independent experiments (n=3).

(J) Statistical analysis of the trypan blue staining of mES cells transfected with *pre-miR-590* and control. Data shown are means ± SD of three independent experiments (n=3).

(K) Statistical analysis of the trypan blue staining of *miR-590*-overexpressed mES cells irradiated by the x-ray. 0 h means staining the cell without time to repair the DNA damage after irradiating. 3 h means staining the irradiated cell after 3 h. Data shown are means ± SD of three independent experiments (n=3).

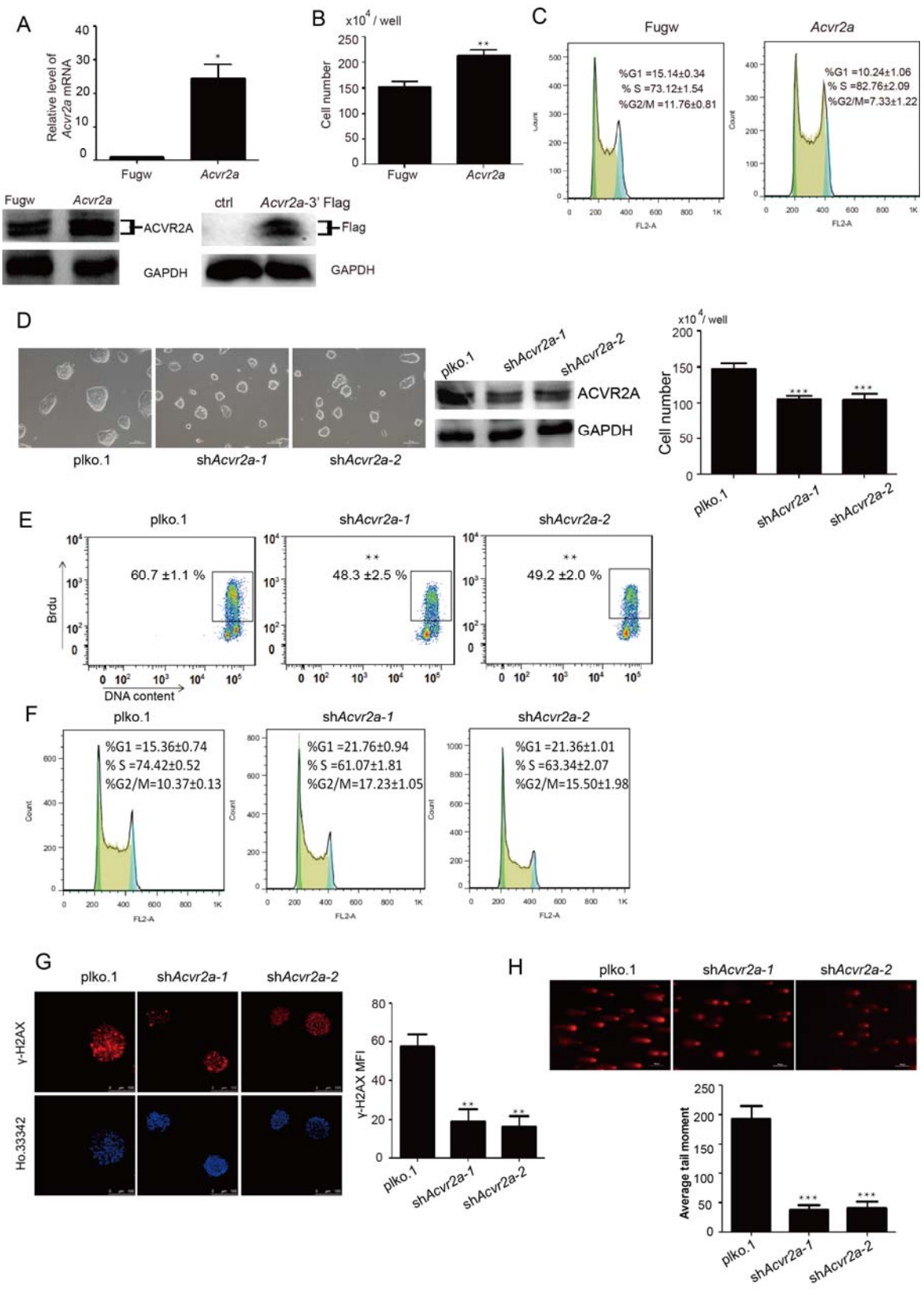

Figure S2

Figure S2, related to Figure 4. Effects of *Acvr2a* on SSB damage repair, DSB

damage repair and proliferation of mES cells

(A) Expression level of *Acvr2a* ectopic expression vector detected by qPCR. Data shown are means ± SD of three independent experiments (n=3). *p < 0.05. Bottom left corner picture showed the effect of overexpression of ACVR2A detected on protein level. Bottom right corner picture showed the bands of *Acvr2a*-flag detected by flag antibody, which determined the two bands of ACVR2A protein.

(B) Counting of amount of the total cells of mES cells overexpressed with *Acvr2a*. Data shown are means ± SD of three independent experiments (n=3). **p < 0.01.

(C) Cell cycle analysis by flow cytometry after propidium iodide (PI) staining. Data shown are means ± SD of three independent experiments (n=3).

(D) Morphology of mES cell clones transfected with sh*Acvr2a-1* or sh*Acvr2a-2* vector. plko.1 is the empty vector. The scale bar represents 100 μm. The effect of the knockdown of *Acvr2a* was detected by western blot. Data shown are means ± SD of three independent experiments (n=3). ***p < 0.001.

(E) Cell proliferation assay by FACS analysis of BrdU labeling. Data shown are means ± SD of three independent experiments (n=3).

(F) Knockdown of *Acvr2a* in mES cells influenced the cell cycle detected by flow cytometry after propidium iodide (PI) staining. Data shown are means ± SD of three independent experiments (n=3).

(G) Immunofluorescence analysis of γ-H2AX (red) to show DSB damage of mES cells. Nuclei were stained with Ho.33342 (Hoechst 33342) (blue). The scale bar

represents 100 μm. Right picture showed the statistical analysis of γ-H2AX mean fluorescence intensity (MFI). Data shown are means ± SD of three independent experiments (n=3). **p < 0.01.

(H) The comet assay shows that knockdown of *Acvr2a* inhibits SSB damage. The scale bar represents 100 μm. The bottom image is the statistical analysis of average tail moment of the mES cells. Data shown are means ± SD of three independent experiments (n=3). ***p < 0.001.

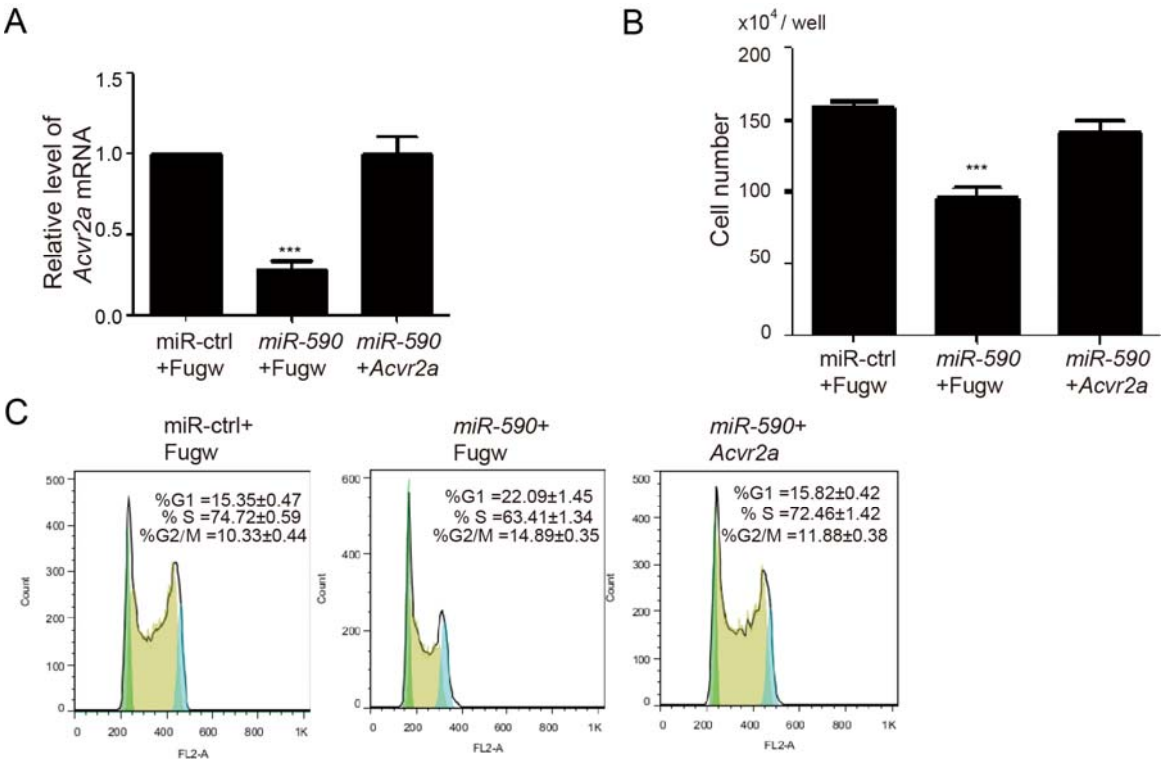

Figure S3

Figure S3, related to Figure 4. *Acvr2a* rescues the function of *miR-590* on cell proliferation and cell cycle

(A) *Acvr2a* expression in the rescue experiment detected by qPCR. Data shown are means ± SD of three independent experiments (n=3). ***p < 0.001.

(B) Counting of total amount of mES cells. Data shown are means ± SD of three independent experiments (n=3). ***p < 0.001 .

(C) Cell cycle analysis by flow cytometry after propidium iodide (PI) staining. Data shown are means ± SD of three independent experiments (n=3).

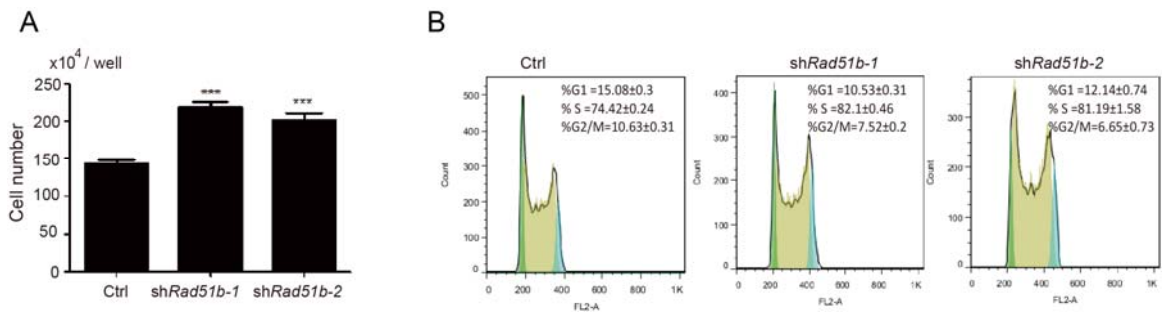

Figure S4

Figure S4, related to Figure 5. Knockdown of *Rad51b* promotes the proliferation

(A) Counting of total amount of mES cells after *Rad51b* knockdown. Data shown are means ± SD of three independent experiments (n=3). ***$p < 0.001$.

(B) Cell cycle analysis by flow cytometry after propidium iodide (PI) staining. Data shown are means ± SD of three independent experiments (n=3).

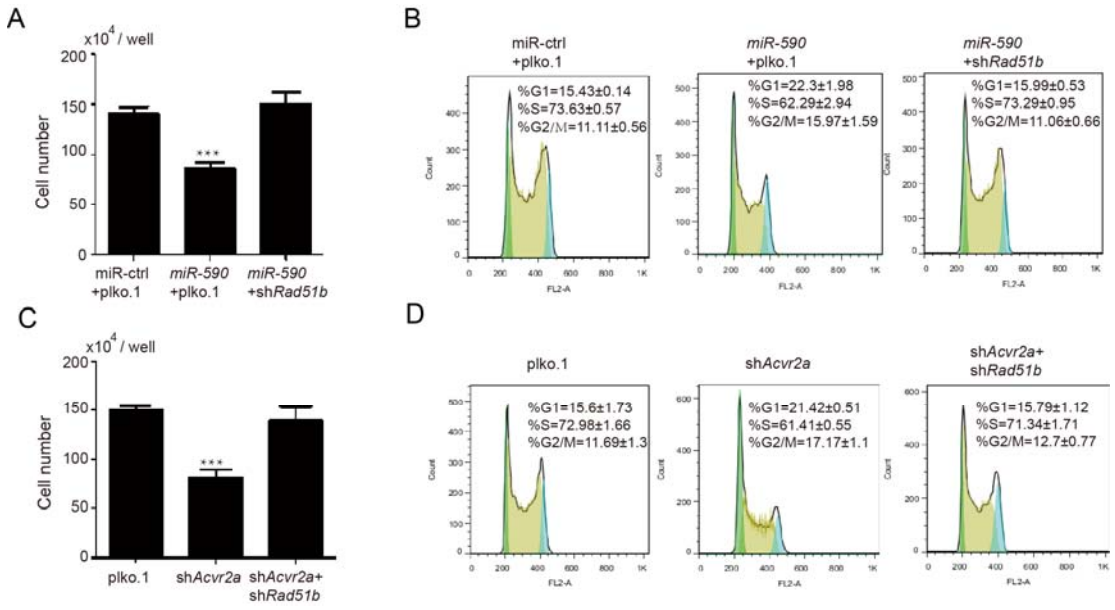

Figure S5

Figure S5, related to Figure 6. *miR-590/Acvr2a/Rad51b* axis regulates the proliferation and cell cycle of mES cells

(A) Counting of total amount of mES cells in the rescue experiment between *miR-590* and *Rad51b*. Data shown are means ± SD of three independent experiments (n=3). ***$p < 0.001$.

(B) Cell cycle analysis of mES cells in the rescue experiment between *miR-590* and *Rad51b* by flow cytometry after propidium iodide (PI) staining. Data shown are means ± SD of three independent experiments (n=3).

(C) Counting of total amount of mES cells in the rescue experiment between *Acvr2a* and *Rad51b*. Data shown are means ± SD of three independent experiments (n=3). ***$p < 0.001$.

(D) Cell cycle analysis of mES cells in the rescue experiment between *Acvr2a* and

Rad51b by flow cytometry after propidium iodide (PI) staining. Data shown are means ± SD of three independent experiments (n=3).